Eidgenössische Technische Hochschule Zürich
Swiss Federal Institute of Technology Zurich

Institute of Biomedical Engineering
Prof. Dr. Klaas P. Prüssmann
Chair of Cognitive Science
Prof. Dr. Christoph Hölscher
Dr. Victor Schinazi
Spring Semester 2018

M.Sc. Thesis

Predicting spatial navigation abilities in humans using shape analysis of the hippocampus

Arda Dogan

October 8, 2018

Supervisors: Dr. Victor Schinazi
Prof. Dr. Christoph Hölscher
Co-supervisor: Prof. Dr. Klaas Prüssmann

Abstract

Humans and animals can use place or response learning to navigate. Place learning is associated with storing a spatial representation of the environment and is governed by the hippocampus. In contrast, response learning is manifested by acquiring reliable sequence of responses and is mediated by the caudate. However, the relationship between the hippocampus and the caudate is not fully understood. Hartley and Burgess (2005) proposed three possible ways of interaction between these two mediators. Competition occurs when they drive conflicting responses in a navigation task. Cooperation occurs when either of these structures is recruited according to the given task. Compensation occurs when one of the two structures is functionally impaired, resulting in the recruitment of the other. The goal of this Masters work is to investigate the relationship between the hippocampus and the caudate using local shape analysis and machine learning methods.

In this work we report the results of an experiment that involved two Virtual Reality (VR) tasks. In one task twenty participants were trained with an arrow whereas a map was used on the other task. Subjects were also tested without a navigation aid and the time scores in training and test trials in both tasks were recorded. Then, the participants' hippocampi and the caudates were bilaterally segmented from T1-weighted Magnetic Resonance (MR) images. Next, Spherical Harmonics (SPHARM) coefficients were extracted as local descriptors and used as features in support vector machines (SVM) classification to assess the subcortical structures' ability of predicting the behavioral scores. Furthermore, statistically significant regions were investigated with global statistical analysis using the Voxel Based Morphometry (VBM) and local statistical shape analysis using the Multivariate Analysis of Covariance (MANCOVA).

Classification results showed that the left hippocampus predicted the participants' ability to learn during map task training trials with 74.9% accuracy and the right caudate predicted the map task test trial scores with 73.5% accuracy. The VBM analysis revealed a positive correlation in the posterior and negative correlation in the anterior regions of the left hippocampus with the map task learning scores. Negative correlation in the head of the right caudate with the map task test scores was also observed. Local statistical analysis results agreed with the VBM results but also provided exact locations of the volume changes. This Masters work showed a competitive relation between the hippocampus and caudate and proposed a novel way to observe localized shape changes in these structures.

Abbreviations

AD - Alzheimer's Disease

CV - Cross Validation

EEG - Electroencephalography

fMRI - Functional Magnetic Resonance Imaging

FSL - Oxford Centre for Functional Imaging of the Brain (fMRIB)'s Software Library

GPS - Global Positioning System

HD - Huntington's Disease

JRD - Judgment of Relative Direction

MANCOVA - Multivariate Analysis of Covariance

MCI - Mild Cognitive Impairment

MRI - Magnetic Resonance Imaging

MVPA - Multivoxel Pattern Analysis

RBF - Radial Basis Function

SPHARM - Spherical Harmonics

SPHARM-PDM - Spherical Harmonics Point-Distribution Model

S-R - Stimulus-Response

SVM - Support Vector Machines

SVM-RFE - Support Vector Machines-Recursive Feature Elimination

VBM - Voxel Based Morphometry

VR - Virtual Reality

Contents

1 Introduction **6**

2 Theoretical Background **11**

2.1 Behaviorism vs. Cognitivism in Psychology 12

2.2 Place Learning 14

2.2.1 Place Learning in Animals 14

2.2.2 Place Learning in Humans 15

2.3 Response Learning 19

2.3.1 Response Learning in Animals 19

2.3.2 Response Learning in Humans 20

2.4 Hippocampus - Caudate Relationship 21

2.4.1 Competition 22

2.4.2 Cooperation 22

2.4.3 Compensation 22

2.5 Clinical Alzheimer's Disease Studies 23

3 Materials and Methods **25**

3.1 The VR Experiment 25

3.1.1 Participants 25

3.1.2 Materials 26

3.1.3 Procedure 27

3.2 Image Preprocessing 28

3.3 SPHARM Decomposition 30

3.3.1 Mathematical Description of SPHARM Decomposition 30

3.3.2 SPHARM-PDM Pipeline 32

3.4 Classification 35

3.4.1 Support Vector Machines (SVM) . . . 35
3.4.2 Two-Nested Cross Validation (CV) . . . 37
3.4.3 Feature Selection . . . 39
3.5 Statistical Analysis . . . 42
3.5.1 Voxel Based Morphometry (VBM) . . . 42
3.5.2 Statistical Shape Analysis using SPHARM-PDM Reconstructed Images . 43
3.6 Complete Workflow . . . 45

4 Results **46**

4.1 Behavioral Data . . . 47
4.2 Classification Results . . . 47
4.3 VBM Results . . . 50
4.3.1 Left Hippocampus . . . 50
4.3.2 Right Hippocampus . . . 51
4.3.3 Right Caudate . . . 51
4.4 Local Statistical Shape Analysis Results . . . 52
4.4.1 Left Hippocampus . . . 53
4.4.2 Right Hippocampus . . . 55
4.4.3 Right Caudate . . . 56

5 Discussion **56**

6 Conclusion **62**

7 References **64**

Appendices **72**

1 Introduction

In the first-half of 20th century, the discipline of Psychology was dominated by stimulus-response (S-R) theories that attempted to explain the animal learning as a reaction to environmental stimulus (Ertmer and Newby, 1993). In animal spatial navigation this approach led researchers to interpret wayfinding solely based on the location of the reward. However, Edward Tolman conducted series of experiments which showed that rats were also capable of learning without explicit rewards. In one of his experiments he blocked the path that the rats were trained to use and then observed that the rats managed to choose a different path that allowed them to shortcut directly to the reward. Tolman concluded that the rats were forming cognitive maps which he defined as the mental representation of the spatial features of the environment in which the animal is navigating (Tolman, 1948). These experiments proved that S-R paradigms were incapable of fully explaining the animal behavior and paved the way for the cognitive revolution of 1960s and 1970s (Miller, 2003).

Tolman's findings motivated scientists in different fields to develop their own experiments within the cognitive framework (Watanabe et al., 2009). In 1971, O'Keefe and Dostrovsky carried out single cell recordings on rat hippocampus in an attempt to find neural correlates of Tolman's cognitive map. They observed that specialized group of neurons fired depending on the rat's position in its environment and called them place cells (O'Keefe and Dostrovsky, 1971). O'Keefe and Dostrovsky concluded that these cells allowed the animal to keep track of its own position while navigating in its environment and that the hippocampus provided animals with a spatial reference map.

In the following years, a number of specialized different cells were discovered. Grid cells in the entorhinal cortex (whose firing pattern resembled a hexagonal lattice) were found to provide an innate coordinate system for the animal (Moser et al., 2008). These cells provided a reference system for the position information encoded by the place cells. Head direction cells in the postsubiculum were found to fire when the animal's head was rotated towards a particular direction (Taube et al., 1990) and border cells in the entorhinal cortex were found to encode the animal's proximity to a border of the room and provided anchor points for grid cells (Solstad et al., 2008). Together with the place cells, grid, head direction and border cells constructed the animal's innate GPS network and formed the basis of allocentric (world-centered) coding.

Similar experiments were done in a quest to discover the existence and neural basis of cognitive maps in human brain. In 2003, Ekstrom and colleagues conducted single cell recording experiments on epilepsy patients while they explored and navigated through a virtual town. They found that some cells had a preferred location and that these cells were concentrated on the hippocampus (Ekstrom et al., 2003). This experiment confirmed the existence of place cells in human brain. Similarly, the existence of grid cells in human entorhinal cortex were confirmed with single cell recording experiments on epilepsy patients while they navigated between four hidden objects in a virtual environment (Jacobs et al., 2013). These experiments proved that a similar navigation system forming the mental representation of the environment existed in humans.

In addition to single cell recording, non-invasive functional neuroimaging and neural recording tools have also been employed to relate the neural activity to navigation tasks. The two most commonly used functional tools in human spatial navigation research are Functional Magnetic Resonance Imaging (fMRI; Hartley et al., 2003; Iaria et al., 2003; Voermans et al., 2004; Suthana et al., 2009; Marchette et al., 2011; Morgan et al., 2011; Vass and Epstein, 2016) and Electroencephalography (EEG; Kahana et al., 1999; Buzsaki, 2005; Ekstrom et al., 2005; Jacobs, 2013). In one landmark study, Hassabis and colleagues (2009) utilized high spatial resolution fMRI and Multivoxel Pattern Analysis (MVPA) in order to decode activity across the population of neurons in human medial temporal lobe while participants navigated in a virtual environment (Hassabis et al., 2009). They managed to show that location information was embedded in the neural activity in the hippocampus. This study demonstrated that the hippocampal activity stored location information and confirmed the role of the hippocampus in human place learning. In another study Vass and colleagues (2016) recorded EEG activity in patients in a VR environment containing teleporters in order to induce motion through space in the absence of visual and self motion cues (Vass et al., 2016). They found that low-frequency oscillations in the hippocampus were elicited during the navigation and sustained even in the absence of visual or self motion cues. This suggested that the activation in the hippocampus was solely related to the location changes inside the environment and reinforced the idea that the hippocampus was the center for human place learning.

High resolution structural MR images have also been employed to relate the behavioral tasks to the volume changes in subcortical structures. The two most common analysis methods in structural MRI studies are the VBM (Maguire et al., 2003; Maguire et al., 2006; Delpolyi et al., 2007; Bohbot et al., 2007; Hartley and Harlow, 2012; Schinazi et al., 2013) and the volumetry (Nedelska et al., 2012; Schinazi et al., 2013). A landmark study on human navigation using anatomical MR images was conducted by Maguire and colleagues (2000) on London taxi drivers (Maguire et al., 2000). In this study, London taxi drivers were chosen as the main subjects of the study because they undergo extensive training and learn how to navigate between thousands of locations in the city. For this reason, they were considered as expert navigators. This study revealed that London taxi drivers, compared to control subjects, had significantly greater gray matter volume in the posterior (tail) region of the hippocampus and less gray matter volume in the anterior (head) region of their hippocampus. This experiment demonstrated that corresponding volume changes were substantially local and solidified the role of the hippocampus in forming the mental representations of the spatial environment.

Second navigation system that involves the consistent performance of a single response to a particular stimulus is apparent in animals. In one study, Packard and McGaugh (1996) bilaterally inactivated the hippocampus and the caudate by means of lidocaine injection (Packard and McGaugh, 1996). They found that the rats whose hippocampus was blocked displayed response learning, whereas the rats whose caudate was blocked displayed place learning. This study demonstrated a second navigation system that governs rodent behavior and that the hippocampus and the caudate were mediators of animal place learning and response learning, respectively.

Neuroimaging studies have shown that similar navigation strategy is also apparent in humans (Hartley et al., 2003; Iaria et al., 2003; Voermans et al., 2004; Maguire et al., 2006; Bohbot et al., 2007). In an fMRI study, Marchette and colleagues (2011) designed a VR experiment that allowed two solutions from two different navigation strategies (Marchette et al., 2011). In the analysis, they compared the hippocampal and caudal activation to the strategy used by participants. They demonstrated that the navigation of humans fell on a continuum from a more flexible cognitive map based strategy centered in the hippocampus to a more rigid route following approach based on the caudate nucleus. This experiment showed that the hippocampus and the caudate were mediators of human place and response learning, respectively.

Although the existence of two navigation systems based on the hippocampus and the caudate is clear, the relationship between these structures is not well-understood. In fact, rats have been shown to utilize all relevant cues in a given maze, suggesting that they are neither inherent "place-learners" nor "response-learners" (Restle, 1957). Three theories have been proposed in order explain their relationship (Hartley and Burgess, 2005). Competition between these two structures occurs when they drive conflicting responses in a navigation task. In a study, Schinazi and colleagues (2013) took sixteen subjects to an unfamiliar university campus and asked them to complete judgement of relative direction (JRD) tasks (Schinazi et. al., 2013). JRDs required participants to assess relative directions of locations and can be regarded as mental shortcuts. For this reason, JRD tasks required the employment of cognitive maps. They used structural MR methods (i.e, the volumetry and the VBM) and found that the JRD errors were positively and negatively correlated with the gray matter volume in the caudate and in the hippocampus, respectively. This study showed a competitive relation between the two mediators since place learning task caused an increase in the hippocampal volume and decrease in the caudal volume.

Cooperation between the hippocampus and the caudate occurs when either one of these structures is recruited according to the given task. In a study Hartley and colleagues (2003) investigated participants using fMRI while they completed tasks specifically tailored to recruit place- and response-based navigation systems (Hartley et al., 2003). They found that successful navigators activated their anterior hippocampus during wayfinding task and head of caudate during route-following task. They concluded that good navigators cooperatively used both navigation systems shifting from one to the other depending on the task.

Compensation between the hippocampus and the caudate occurs when one of the two structures is functionally impaired (due to inhibition or damage) and results in the recruitment of the other. In a study, Voermans and colleagues (2004) investigated response learning abilities in patients with Huntington's Disease (HD) that causes caudal dysfunction (Voermans et al., 2004). They acquired fMRI scans while the participants recalled well-defined routes in a virtual home and observed activity in the hippocampus in a response learning related task. They concluded that the hippocampus compensated for the decreased activity in the caudate due to HD.

In human spatial navigation research, functional and structural neuroimaging methods have been widely employed to understand hippocampus-caudate relationship. In these studies the purpose has been to establish a correlation between the functional and structural properties of the hippocampus and the caudate and the behavioral results obtained from a task. Another possible approach is to infer the results from the anatomical shape changes. Recently, clinical researchers employed this approach using deep learning (Suk et al., 2014) and classification (Li et al., 2007) methods in order to predict Alzheimer's Disease (AD) and Mild Cognitive Impairment (MCI) based on the hippocampal atrophies. In one study Gerardin and colleagues (2009) utilized SVM classification in order to distinguish between AD and MCI patients from healthy control subjects (Gerardin et al., 2009). At the end of the study they achieved over 80% and over 90% classification accuracy in separating MCI and AD patients from controls, respectively. In these studies researchers have used shape analysis and extracted local features to achieve higher accuracy scores. Shape analysis methods are more sensitive to local changes compared to the VBM and the volumetry that gives focus on the global characteristics of the cortical region. Therefore, local shape analysis methods were chosen to acquire higher discriminative power.

Spatial navigation and spatial memory are closely linked to AD and MCI. Impairment in spatial navigation skills has been observed in MCI and AD patients due to the deformation of hippocampal formation (Delpolyi et al., 2007; Nedelska et al., 2012; Vlcek and Laczo, 2014). In addition, Maguire and colleagues have shown that the changes in taxi drivers' hippocampus are substantially local rather than global (Maguire et al., 2000).

In this Masters work, we propose a novel approach to the investigation of hippocampus-caudate relationship from local features rather than behavioral tests. The data used in this work was obtained in a VR experiment where twenty participants were trained in two different tasks specifically tailored for place and response learning and then tested. Firstly, the structural MR images of the participants were registered to a standard space and the hippocampi and the caudates of all participants were segmented. Then hippocampal and caudal shape features were extracted using SPHARM coefficients, i.e. 3D analogous of 2D Fourier series coefficients (Brechbühler et al., 1995). SPHARM decomposition was chosen as the shape analysis method due to its success in classification of AD and MCI patients (Gerardin et al., 2009). After SPHARM coefficients of each participant's hippocampus and caudate were extracted, these features were

utilized in SVM classification with Radial Basis Function (RBF) kernel. However, in order to reduce the bias towards overfitting the data which is high-risk in a small dataset where there are only twenty subjects, the optimization technique was chosen as two-nested Cross Validation (CV). This method has been shown to greatly reduce the bias and give an estimate of accuracy that is very close to that would be obtained by testing on an independent dataset (Varma and Simon, 2006). In addition, the features were ranked using SVM-Recursive Feature Elimination (SVM-RFE, Huang et al., 2014) to increase the accuracy of the classification. Following classification, the performance of each structure's ability to predict six different behavioral tests (place learning initial trial, learning and test; response learning initial trial, learning and test) versus different number of features was observed. Finally, global statistical analysis with the VBM and local statistical shape analysis with the MANCOVA was carried out for behavioral tests that were predicted with high accuracy and hippocampus-caudate relationship was investigated.

In this work, the left hippocampus was shown to achieve 74.5% prediction accuracy on the place learning abilities while the right caudate was shown to achieve 73.5% prediction accuracy on the test trial of place learning task. In addition, the VBM results using these structure-test combinations revealed negative correlation in the head of the right caudate and positive and negative correlations in the tail and the head of the left hippocampus, respectively, indicating a competitive relationship. Furthermore, local statistical analysis showed contractions in the head of the right caudate and left hippocampus, as well as dilations in the tail of the left hippocampus. The local statistical results agreed with the VBM results but also managed to reveal exact locations of these shape changes on these structures.

2 Theoretical Background

This chapter provides a literature review on the place and response learning. The chapter begins with a description of the discipline psychology and a discussion on two main theoretical approaches that have dominated the field in the last century (i.e., behavioral psychology and cognitive psychology). Next, we present research that has uncovered the neural correlates of human and animal place and response learning. Then, we present different theories on the interaction between these two navigation systems. The chapter concludes with a description of another possible approach to investigate the interaction between these two navigation systems.

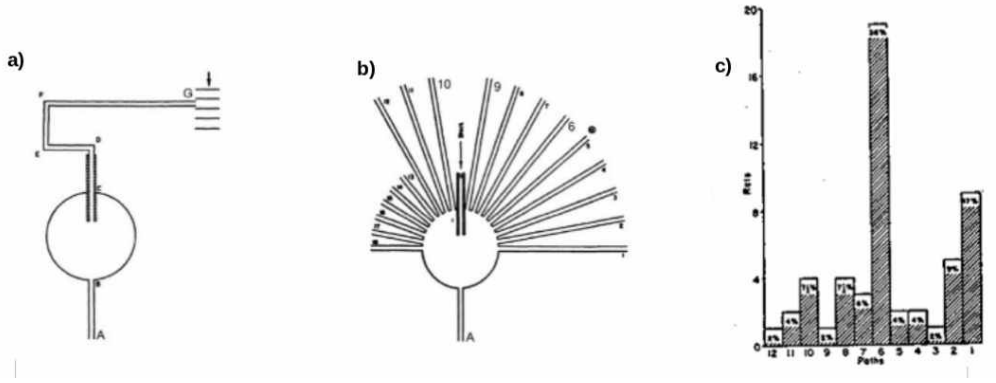

Figure 1: Edward Tolman's experiment on cognitive maps* (Tolman, 1948). **(a)** The initial maze used to train the rats with food reward located at the point G. **(b)** The test maze with the initial path (now blocked) and the 18 alternate paths with different angular orientations into the room. **(c)** The percentage of rats distributed according to the number of path they took. Note that the majority of rats preferred the path number 6 which pointed towards the reward, showing that the rats were capable of forming a mental map of the room. *The resolution of the images are low since they are taken from the original paper published in 1948.

2.1 Behaviorism vs. Cognitivism in Psychology

Psychology is a field of science that investigates the mind and the behavior relationship in animals and humans. Until the 19^{th} century psychology was mainly investigated from a philosophical perspective. In late 1800s, it was separated from its philosophical roots with the inclusion of experimental methods and the first formal laboratory was established in 1879 by Wilhelm Wundt at the University of Leipzig, Germany (Mandler, 2011). The modern psychologists in Germany were mainly investigating consciousness with methods of introspection. In early 1900s, a novel approach in psychology was born in the United States. This new approach was an objective method rejecting the involvement of consciousness, reducing the field to the study of the behavior and extending the subjects to animals as well as humans (Watson, 1913). Numerous researchers around the globe embraced this new approach and consequently behaviorist theories dominated the field in the first half of the 20^{th} century.

Towards the mid 20^{th} century, Edward Tolman carried out series of experiments that showed the inadequacy of stimulus response (S-R) theories explaining learning and behavior. In his landmark experiment, Tolman trained a group of rats in a one-way maze that consisted of a single path towards a food reward. After the training process, he blocked the initial path but

opened 18 different paths at various angular directions one of which lead directly to the reward. He observed that the majority of the rats preferred the path number 6 which allowed them to shortcut directly to the food (Figure 1). Tolman explained this behavior with the concept of cognitive maps which he defined as the mental representation of the environment in which the animal is navigating (Tolman, 1948). According to Tolman, the rats responded to the stimulus by referring to their cognitive maps and managed to choose an alternate path that allowed them to directly reach the reward.

Tolman's experiments were considered as a turning point in the discipline of psychology (Miller, 2003). Behavioral psychologists suggest that learning occurs as a sequence of habitual responses due to a particular stimulus during training (Watson, 1913; Skinner, 1953). Tolman's experiments demonstrated that the rats did not display a direct motor response to the stimulus and were capable of building mental representations during the learning process. His experiments showed that behaviorist theories were not capable of fully explaining the animal behavior and originated cognitive psychology. Cognitive theories suggest that the learning does not occur as simple reactions to environmental stimuli and a cognitive process is involved. This cognitive layer between the stimulus and the response involves all processes by which the sensory input is transformed, reduced, elaborated, stored, recovered, evaluated and used (Neisser, 1967). Therefore, while behaviorist approaches suggest a rigid connection between the stimulus and the response, cognitive theories propose the involvement of cognition that enables flexible actions (Figure 2).

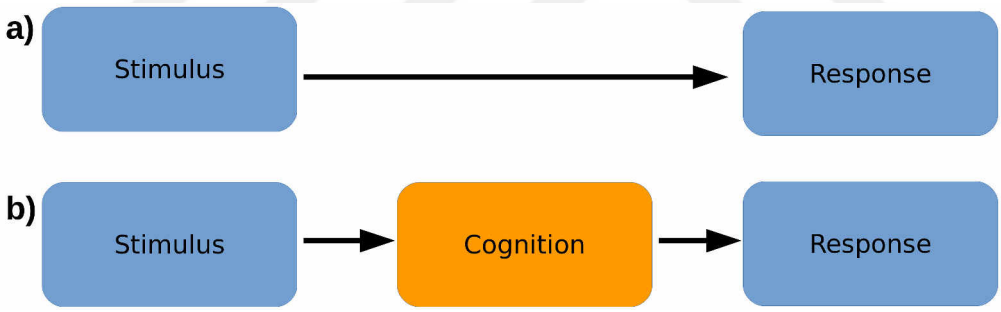

Figure 2: **(a)** Behaviorist approach to psychology. The response is purely seen as a reaction to given stimulus. The connection between stimulus and response is rigid. **(b)** Cognitivist approach to psychology. There is a cognitive layer in between the stimulus and the response which consists of all processes by which the sensory input is transformed, reduced, elaborated, stored, recovered, evaluated and used. Cognition allows for less rigid connection and flexible actions.

2.2 Place Learning

Spatial navigation within the cognitive framework stems from the idea of cognitive maps proposed by Edward Tolman. According to this theory, animals and humans store spatial information and build a mental map of their environment. These mental representations allow for the development of novel and flexible routes during navigation. This navigation system is referred as place learning and animals and humans that display flexible navigation are called place learners.

2.2.1 Place Learning in Animals

Tolman's findings motivated scientists to investigate the neural correlates of place learning in both animals and humans. In 1971, O'Keefe and Dostrovsky carried out single cell recording experiments on the hippocampus of rodents. Their work was motivated from previous findings that showed that animals with hippocampal damage exhibited poor navigation performance (Douglas, 1967; Kimble, 1968; Morris, 1984). O'Keefe and Dostrovsky discovered the existence of place cells in the rat's hippocampus that fired depending on the rat's position in the environment (O'Keefe and Dostrovsky, 1971). Each of these cells had its own place field that determines its firing rate depending on the animal's location (Muller, 1996; Figure 3a). Considering that there are numerous place cells in the hippocampus, the collective firing rate of these cells can encode the animal's exact location in its environment. For this reason, O'Keefe and Dostrovsky reasoned that the hippocampal area might provide the animals with a cognitive map of their environment.

The discovery of place cells in rodent hippocampus motivated the researchers to focus their studies on the hippocampal region. In 2005, Hafting and colleagues discovered a group of cells in entorhinal cortex that fired in certain locations of the room but irrespective of the animal's own location (Hafting et al., 2005). They observed that the firing pattern of these cells produced a hexagonal grid covering the entire environment. They concluded that this grid structure constituted an innate coordinate system inside the animal's brain and provided reference for the position information encoded by the place cells. Researchers have also discovered head direction cells in the postsubiculum (Taube et al., 1990) and border cells in the entorhinal cortex (Solstad et al., 2008). These cells encoded the facing direction of the animal and the geometric boundaries of the environment, respectively. Together all these cells constructed the animal's innate GPS network and constituted the neuroanatomical foundations of animal place learning.

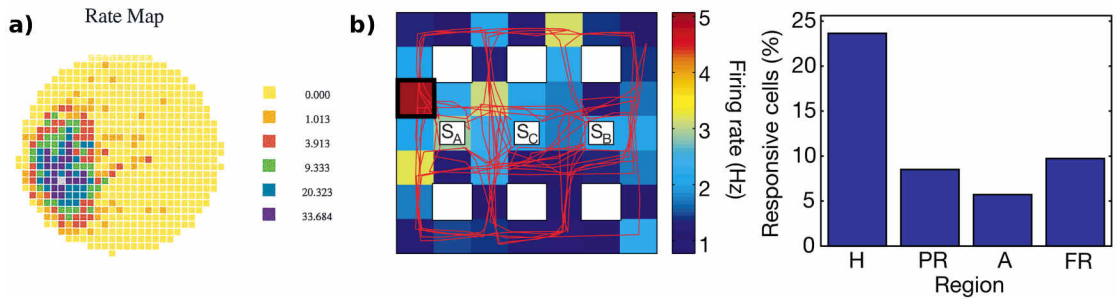

Figure 3: Place cells in animals and humans. **(a)** The place field of a single cell in rodent hippocampus which shows the firing rate of the cell in different locations inside the environment (O'Keefe and Dostrovsky, 1971; Muller, 1996). The sensitivity of the cell is distributed around a preferred location where the cell's firing rate peaks. **(b)** Single cell recording experiment on epilepsy patients while navigating through a virtual town (Ekstrom et al., 2003). Left: Firing rate of a right hippocampal cell as shown in a grid representing the virtual town while the red lines show the patient trajectory. The red square shows the location of where the firing rate of this neuron is peaked, demonstrating place sensitivity. Right: Distribution of place sensitive cells in hippocampus (H), parahippocampal region (PR), amygdala (A) and frontal lobe (FR). The cells which are responsive to certain location in the space are clumped up in the hippocampus.

2.2.2 Place Learning in Humans

Ekstrom and colleagues (2003) conducted single cell recording experiments on epilepsy patients while the patients navigated through and explored a virtual town (Ekstrom et al., 2003). In this study, they recorded from 317 different neurons in hippocampus, amygdala, parahippocampal region and frontal lobes. They found that place responsive cells were clustered in the hippocampus (Figure 3b). They concluded that these cells constituted the homologous of place cells observed in rat hippocampus by O'Keefe and Dostrovsky (1971) and that the hippocampus was central to human place learning.

In addition to the place cells, the existence of grid cell in human entorhinal cortex were confirmed with single cell recording experiments on epilepsy patients while they navigated between four hidden objects in a virtual environment (Jacobs et al., 2013). The presence of place and grid cells in the human hippocampal formation indicated the existence of a similar navigation system in human brain.

Following the confirmation of place and grid cells in human hippocampal formation, researchers focused on human hippocampus in order to investigate the neural correlates of human place learning. In addition to the single cell experiments, non-invasive neuroimaging and neural recording tools were also employed in functional (using fMRI and EEG) and structural (using

anatomical MR images) studies. While functional studies investigated the activity observed in cortical regions during a behavioral task, structural studies focused on correlations between the gray matter volume changes in subcortical structures and behavioral performances in tasks.

Functional MRI measures the neural activity during a task utilizing the changes in magnetic susceptibility differences between oxygenated and deoxygenated hemoglobin. During a task tailored to induce brain activity in a certain region, the fresh blood rushes to carry oxygen to neurons in that area which causes a signal increase. This type of contrast achieved in an fMRI study is called the Blood-Oxygenation-Level-Dependent (BOLD) response and is an indicator of a neural activity in a particular region during a neural task.

Navigation studies on humans have commonly employed fMRI to investigate the correlation between the hippocampal activity and the behavioral tasks (Hartley et al., 2003; Iaria et al., 2003; Voermans et al., 2004; Suthana et al., 2009; Marchette et al., 2011; Morgan et al., 2011; Vass and Epstein, 2016). In one fMRI study, Hassabis and colleagues (2009) asked participants to navigate in two virtual rooms and reach four different target positions located at the corners of the rooms (Hassabis et al., 2009). They scanned the participants when they reached the targets in order to isolate location information. They used Multi Voxel Pattern Analysis (MVPA) which is a supervised classification method to capture the relationships between spatial patterns of fMRI activity and experimental conditions (Mahmoudi et al., 2012). Hassabis and colleagues managed to show that the location information of participants was manifested in the hippocampal activity using classification accuracies (Figure 4a). This study showed that the hippocampal activity encoded the location information of the participants during navigation and confirmed the central role of the hippocampus in human place learning.

Electroencephalography (EEG) is a neural recording method used to measure the evoked potentials from the correlated synaptic activity and postsynaptic potentials in cortical neurons (Niedermeyer and Da Silva, 2005). EEG devices consist of set of electrodes that are placed on top of the scalp and record electrical activity during a specific task. EEG signals are categorized based on the frequency of the observed signal; Delta waves (less than 4 Hz), Theta waves (4-7 Hz), Alpha waves (7-15 Hz), Beta waves (16-31 Hz) and Gamma waves (greater than 32 Hz).

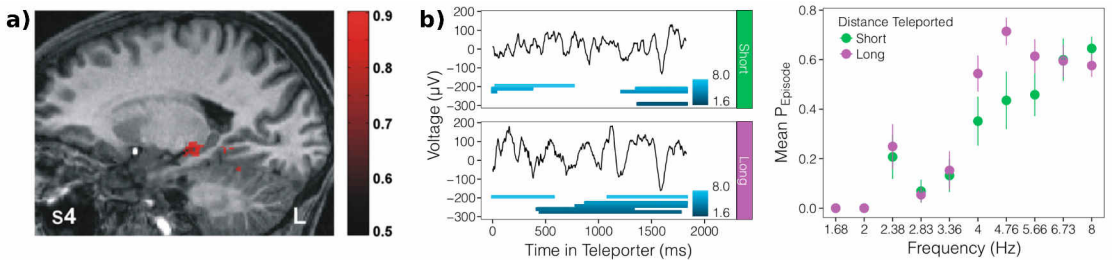

Figure 4: Functional studies in human place learning. **(a)** Pairwise position prediction map of a participant using the fMRI signal activites and the targets in MVPA classification displayed on a structural MR image in a sagittal view* (Hassabis et al., 2009). Voxels in the body-tail regions of the hippocampus display accuracy results over 50% which was regarded as significantly above chance. This showed that the spatial information was encoded with the hippocampal activity. *The colorbar indicates a percentage accuracy values with a threshold set at 66.07%. **(b)** Application of EEG in spatial navigation research as observed from an example electrode (Vass et al., 2016). Left: Raw traces obtained from EEG recording during long and short teleportation, showing that navigation without any sensory information induced low frequency band delta and theta waves. Right: Mean proportion of time at each frequency during short and long teleportation. Separation between long and short teleportation was apparent, showing that the information of distance was encoded in the frequency of the signal.

In human place learning research, EEG has been used to observe low frequency theta and delta waves in the hippocampal local field potential (Kahana et al., 1999; Buzsaki, 2005; Ekstrom et al., 2005; Jacobs, 2013). In one study, Vass and colleagues (2016) recorded EEG activity in patients in a VR environment containing teleporters in order to induce motion through space in the absence of visual and self motion cues (Vass et al., 2016). They found that low-frequency oscillations in the hippocampus were elicited during the navigation and sustained even in the absence of visual or self motion cues. They concluded that the activation in the hippocampus was independent of visual or motion cues and was solely related to the location changes inside the environment. In addition, they demonstrated that these waves carried meaningful spatial information by decoding distance traveled from the waves and relating the frequency of the observed waves to the distance traveled in short and long distance teleporters (Figure 4b). This study showed that the hippocampal activity carried location and distance information and that the hippocampus had a crucial role in storing spatial data.

Structural MR studies, on the other hand, relate navigational abilities to subcortical structures through gray matter volume changes. The two most commonly employed methods to observe correlations between the volume changes and the behavioral scores are the volumetry and the VBM.

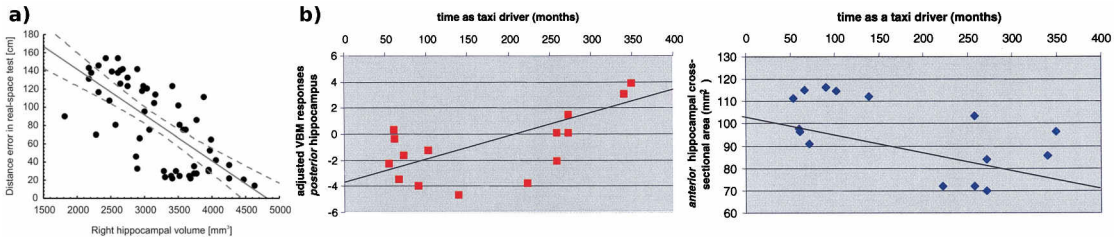

Figure 5: Structural studies in human place learning. **(a)** Distance error versus right hippocampal volume obtained with the volumetry (Nedelska et al., 2012). Negative correlation between the distance error made by the subjects and their right hippocampal volume indicated that the better place learners had larger right hippocampi. **(b)** Structural MR study on London taxi drivers obtained with the VBM method (Maguire et al., 2000). Left: Volume of the right posterior hippocampus shows positive correlation with the time spent as taxi driver. Right: Volume of the right anterior hippocampus shows negative correlation with the time spent as taxi driver. These results implicate that place learning abilities cause local changes in gray matter volume.

In the volumetry, a certain region of interest is specified and segmented. Next, the number of voxels in that region or its subregions are counted. Then, the volume differences are related to the participants and their performances. Volumetry has been used in spatial navigation research to relate the hippocampal volume changes to place learning tasks (Maguire et al., 2000; Schinazi et al., 2013). One study that used the volumetry was conducted by Nedelska and colleagues (2012) where the navigation abilities of AD and MCI patients were compared to healthy controls of similar age (Nedelska et al., 2012). In the study, they used a real-space human analog of the Morris water maze where participants were required to swim to find hidden platforms (Morris, 1984). They carried out a volumetric analysis on right hippocampus and showed that there is a negative correlation between the errors made during a way-finding task and the right hippocampal volume (Figure 5a). This study showed that decreased volume in the right hippocampus of AD and MCI patients resulted in a poor spatial navigation performance.

While the volumetry requires a priori information about the structure for regional analysis, the VBM provides a voxel wise statistical analysis in the overall brain and indicates all regions that are potentially related to the behavioral performance. The VBM has been widely used in previous research to find correlations between the gray matter volume and human place learning (Maguire et al., 2003; Maguire et al., 2006; Delpolyi et al., 2007; Bohbot et al., 2007; Hartley and Harlow, 2012; Schinazi et al., 2013). One landmark study regarding the human spatial navigation using anatomical MR images and the VBM was conducted by Maguire and colleagues on London taxi drivers (2000). London taxi drivers were chosen as the main subjects of the study because

they were considered expert navigators since they are required to undergo extensive training and learn how to navigate between thousands of locations in the city. Findings from this study revealed that, compared to control subjects, London taxi drivers had significantly more gray matter volume in the posterior region of the hippocampus. In addition, they demonstrated a negative correlation between the gray matter volume in the right anterior hippocampus and the time spent as a taxi driver (Figure 5b). This study reinforced the idea that the hippocampus was central in human place learning and further showed that the volume changes in hippocampus due to place learning abilities were substantially local rather than global.

2.3 Response Learning

Response learning is manifested by sequence of actions in response to a certain stimulus (e.g., turn left at the church). This type of learning leads to a habitual navigation that is more rigid compared to flexible place learning. This navigation system is called response learning and subjects that displays habitual navigation are called response learners.

2.3.1 Response Learning in Animals

Packard and colleagues (1989) conducted a series of lesion and injection studies to investigate the neural correlates of the response learning. In a study using 8-arm radial maze, they placed the food reward once at each arm which was consistently paired with a light cue and compared the errors made by control group and rats with caudal lesion (Packard et al., 1989). They observed that the rats with caudal lesion displayed greater number of errors compared to the control group. They concluded that these rats were impaired in responding to a stimulus compared to control subjects and that the caudate played a central role in response learning.

In one landmark study, Packard and McGaugh (1996) bilaterally inactivated the hippocampus of one rat group and the caudate of another group with lidocaine. A third group of healthy rats were injected with a saline solution and used as controls (Packard and McGaugh, 1996). In this sixteen day experiment, they trained the rats in days 1-7 and 9-15 and carried out probe trials on days 8 and 16. They observed that the group with caudal injection displayed place learning on both trials while the group with hippocampal injection displayed response learning only on the second trial (Figure 6). At the end of the study, they reported three main findings. First

they concluded that the caudate and the hippocampus were the centers for response and place learning, respectively. Second, they observed that the place learning was employed on the first probe trial whereas the response learning was apparent only on the second probe trial. Third, they demonstrated that the place learning stayed intact after the rats switched to response learning.

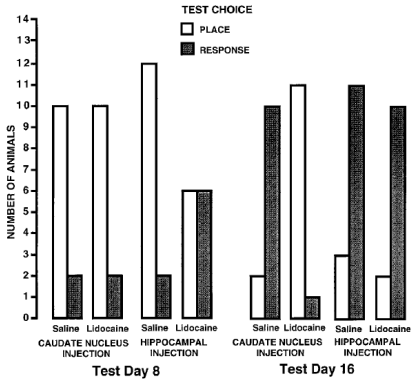

Figure 6: The effect of functional inactivation of the hippocampus and the caudate on place learning and response learning navigation systems (Packard and McGaugh, 1996). Control group of rats with saline injection showed place learning on day 8 and response learning on day 16, indicating the earlier recruitment of the place learning navigational system. Group of rats with caudal lidocaine injection displayed place learning on both day 8 and day 16, showing that the place learning continued to function if the response based navigation system was blocked. Group of rats with hippocampal lidocaine injection showed neither response nor place learning but displayed response learning on day 16.

2.3.2 Response Learning in Humans

Functional neuroimaging studies have shown that a similar response system mediated by the caudate nucleus may also be present in humans (Voermans et al., 2004; Marchette et al., 2011). In one fMRI study Hartley and colleagues (2003) designed a virtual reality experiment in which the participants were required to complete two tasks. In one task participants were asked to explore the virtual town. In the other task, participants were trained to follow a fixed route. After the training, they tested participants' ability to find novel shortcuts in the first town and to follow a familiar route in the other. They carried out a between subject analysis to find the neural correlates underlying the performances observed in the experiment. Their findings revealed that the head of the right caudate was active when participants followed a fixed route. In addition, the results demonstrated that the perirhinal cortex of hippocampal formation was activated during the wayfinding task. This study confirmed the navigation system based on response learning governed by the caudate nucleus and also showed the coexistence of place and response learning in human brain.

In another fMRI study, Iaria and colleagues (2003) designed an experiment with virtual 8-arm maze in front of a landscape. In each trial, they placed four objects at the end of four different locations to be picked up. In addition, the landscape behind the maze was hidden by walls in the probe trials (Iaria et al., 2003). They observed increased activity in the hippocampus of the participants who navigated to the target objects using the spatial relations between the arms and the landscape. Furthermore, the results also revealed an increased activity in the caudate nucleus of participants that preferred nonspatial strategy (i.e., counting the arms to navigate). Their findings verified that the hippocampus mediated place learning in humans while the caudate governed the human response learning.

Previous research have also used structural MR images to investigate the caudate nucleus and the response learning (Maguire et al., 2006). Bohbot and colleagues (2007) used a virtual 8-arm radial maze in a landscape to investigate volume changes due to different navigation strategies. In this experiment, they placed four objects at the end of four arms and participants navigated using direction commands (i.e., forward, left and right arrow keys) from the keyboard (Bohbot et al., 2007). In the probe trial the landscape was removed to distinguish between the place and response learners from the errors made in the probe trial (i.e, more errors without landscape indicated a spatial strategy). They observed using the VBM analysis that the caudal volume correlated negatively with the errors while positive correlation was apparent in the hippocampal volume. This study reinforced the idea that place and response learning in humans were governed by the hippocampus and the caudate, respectively.

2.4 Hippocampus - Caudate Relationship

While the two different navigation systems governed by the hippocampus and the caudate are apparent in both humans and animals, their relationship is not fully understood. In fact, rats have been shown to utilize all relevant cues in a given maze, suggesting that they are neither inherent place learners nor response learners (Restle, 1957). Following the ideas from previous studies, Hartley and Burgess categorized the relationship between the hippocampus and the caudate into three theories (Hartley and Burgess, 2005). These theories are called competition, cooperation and compensation.

2.4.1 Competition

Competition between these two systems occurs when both systems compete to control the behavior in a navigation task. One study that demonstrated the competitive relationship was conducted in 2013 by Schinazi and colleagues in which they took sixteen subjects to an unfamiliar university campus and asked them to complete four different navigational tasks (Schinazi et al., 2013). One of these tasks required the participants to make judgments of relative direction (JRDs). In JRD tasks participants were asked to evaluate the direction of a location in space relative to a given reference point (can be regarded as mental shortcuts). For this reason, completing these tasks required the use of participants' mental representations of the campus. After the task, T1-weighted MR images of the participants were taken and both the volumetry and the VBM analyses were carried out to relate the JRD errors to volume changes in cortical structures. They found that the errors had positive correlation with the right caudate and negative correlation with the right hippocampus. The findings from this study indicated a competitive relation between these two systems.

2.4.2 Cooperation

Cooperation between the two navigation systems occurs when either one of these systems is recruited during a navigation depending on the task. In an fMRI study by Hartley and colleagues (2003) participants were required to complete two different tasks tailored to activate the hippocampus and the caudate (Hartley et al., 2003; refer to section 2.3.2 for the description of the experiment). In this study, they also carried out within subject analysis and observed activity in the hippocampus during wayfinding task and in the caudate during route-following task in accurate navigators' brain. They concluded that accurate navigators were capable of utilizing both systems and switching from one to the other depending on the task. This study indicated a cooperative relationship between the hippocampus and the caudate.

2.4.3 Compensation

Compensation between the two navigation systems occurs when one system is functionally unavailable which leads to the recruitment of the other system. One study that showed the compensation relationship was carried out by Voermans and colleagues (2004) on participants with caudate nucleus dysfunction caused by Huntington's disease. (Voermans et al., 2004). In this

study, participants were scanned while they were recalling well-defined routes that they learned in virtual homes. At the end of the study, the authors observed that while the less severely impaired patients showed greater activity in the caudate nucleus as expected, participants with severe dysfunction displayed more activity in bilateral hippocampus. They concluded that the hippocampus was recruited in the patients whose caudate nucleus was not functioning properly and compensated for the decrease in the caudal activity.

2.5 Clinical Alzheimer's Disease Studies

Previous studies investigated the hippocampus-caudate relationship using neuroimaging studies and tried to infer their functions using statistical methods from the observed behavior during experiments. Another approach is to look at the relationship between these cortical structures using their local features and to infer the behavioral performances. This approach has been commonly used in clinical diagnostic research. Clinical research constructs a model that distinguishes patients from healthy subjects using anatomical atrophies. This approach has been commonly used in research on AD since there is no general consensus on its behavioral indicators.

Recently, researchers have employed machine learning methods such as deep learning (Suk et al., 2014) and classification methods (Li et al., 2007). In these studies, cortical structures that are known to be affected by the disease are determined and their features are extracted using shape analysis methods. Shape analysis has been commonly used since these methods are more sensitive to local cortical changes compared to the volumetry and the VBM and since conditions such as AD is manifested throughout local regional shape changes (Chan et al., 2016). Furthermore, local shape descriptors obtained from shape analysis methods are used to construct machine learning models that aims to carry out high accuracy diagnosis.

In one study, Gerardin and colleagues (2009) collected anatomical MR data of AD and MCI patients as well as healthy control subjects (Gerardin et al., 2009). After the scan they extracted local shape descriptors from the left and right hippocampus using spherical harmonics (SPHARM) method and utilized SPHARM coefficients as features in SVM classification. Furthermore, they employed linear and radial basis function (RBF) kernels for comparison purposes. They managed to separate AD and MCI patients from healthy control subjects with 94% and 83% accuracies using RBF kernel, respectively (Figure 7).

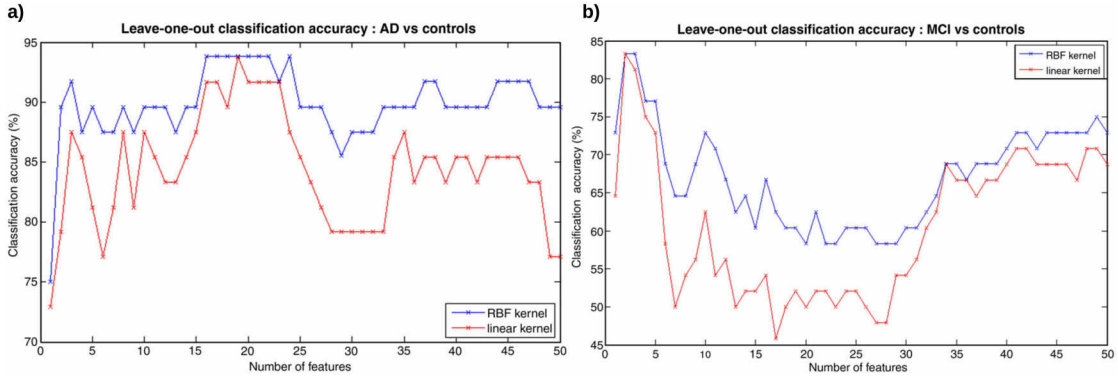

Figure 7: Classification accuracies in distinguishing **(a)** AD patients and **(b)** MCI patients from healthy controls utilizing the shape features of left and right hippocampus (Gerardin et al., 2009). Accuracy results for both linear and RBF kernel is shown. Classification accuracy reaches 94% for AD using 16-22 features and 83% accuracy is obtained for MCI using 1-2 features with RBF kernel.

Previous research has shown that the navigation is mediated in animals and humans by two different navigation systems. Place learning (centered in the hippocampus) allows for storing and evaluating spatial information and developing flexible routes during navigation. Response learning (governed by the caudate nucleus) is manifested by sequence of actions in response to a certain stimulus that leads to habitual and more rigid navigation. The relationship between these two systems have not been fully understood. In this study, we aim to to investigate the relationship between the hippocampus and the caudate using the ideas inspired by the clinical AD studies that utilized machine learning methods. We believe that this approach might shed a new light on these two navigation systems for two reasons.

First, the AD and MCI are related to memory loss and atrophies observed in the hippocampus. Cognitive spatial navigation is closely linked to spatial memory in the hippocampus and impairment of place learning abilities were observed in AD and MCI patients as they displayed poor navigation performances in place learning tasks (Vlcek and Laczo, 2014; Nedelska et al., 2012). Since both AD and place learning have the same neural correlates, we believe that the same methodology can be applied to yield deeper insight.

Second, diagnostic AD and MCI studies utilize local shape features in classification algorithms since the effects of AD and MCI are manifested throughout local regions of the hippocampus

(Li et al., 2007; Gerardin et al., 2009; Chan et al., 2016). Previous research has shown that the effects of place and response learning are also manifested locally rather than globally. Previous studies have demonstrated that the correlations between the place learning abilities and the posterior and the anterior hippocampus are positive and negative, respectively (Maguire et al., 2000; Bohbot et al., 2007; Schinazi et al., 2013). In addition, response learning abilities have been shown to correlate positively predominantly with the head of the caudate nucleus (Hartley et al., 2003; Bohbot et al., 2007). Therefore, we believe that the approach used in clinical AD studies that utilizes local features has the potential to reveal further information about the role of the hippocampus and the caudate in human spatial navigation.

3 Materials and Methods

This section provides the detailed description of the materials and the methods used to analyze the collected data. The section begins with a description of the experiment. Next, the preprocessing pipeline for the segmentation of the participants' hippocampi and caudates from the structural MR images is briefly described. This is followed by a detailed description of the SPHARM decomposition method used for feature extraction. Then, the SVM classification, the two-nested CV algorithm and feature selection through SVM-RFE are described. Finally, the statistical shape analysis methods using the VBM and SPHARM-Point Distribution Model (SPHARM-PDM) reconstructed images with the MANCOVA are explained.

3.1 The VR Experiment

3.1.1 Participants

Twenty-four participants were recruited for the experiment and four participants were excluded from the analyses due to simulator sickness. The age of the remaining twenty participants (10 female) were ranged from 19 to 38 with a mean age of 25.

The experiment was approved by the ETH Zurich Ethics Commission (EK 2013-N-73). Prior to starting the experiment, written informed consent was obtained from all participants. The participants were paid 30 CHF per hour. Participants that aborted the experiment due to simulator sickness were compensated with 20 CHF.

3.1.2 Materials

The technical setup for the experiment consisted of a WorldViz CAVE setup with three computers. Each system was equipped with a Core i7-3820 at 3.6 GHz with 12 GB of RAM and an Nvidia Quadro K4000 with 3 GB RAM. The CAVE consisted of three ultra short throw projectors NEC U310W running at a 1680 x 1050 resolution during 3D projection. To enable 3D perception, alternate frame sequencing shutter glasses of the type Volfoni 3DGE RF were used. The WorldViz PPT Real-Time Motion Tracking System was used for tracking head position and orientation. The tracking system was connected to a separate computer to reduce the computational load on the main machines. Participants were seated in a chair that was located in the middle of the CAVE facing towards the middle screen. A small table was mounted on the arm rests to comfortably place the joystick (Logitech Extreme 3D Pro) for the participants.

The motion sensors attached to the participants' head was used to determine the participants' orientation in the virtual environment and provided the orientation of the participant with respect to the CAVE. Participants used both the head orientation and the joystick to turn and move within the virtual environment. Twisting the joystick left or right and turning the head provided rotations whereas translational movements (i.e., forward, backward, left, and right) were executed by pushing the joystick in the desired direction. However, there was a subtle difference in how the joystick and head trackers were used to control rotation. Motion sensors in the head changed only the virtual direction from which the observer's viewing direction is recorded while with the joystick the projected virtual environment was rotated. A visual "catchment area" was provided in order to facilitate the interaction with elements in the environment. This catchment area consisted of a yellow semi-transparent circle on the ground that moved with the participant's position and head rotation (yaw axis) to indicate the location where we consider an interaction to occur. All translational movements were performed relative to the viewing direction (i.e., pushing the joystick forward always resulted in the expansion of optic flow from the point of focus).

Custom-designed software (Grübel, 2014) was used for conducting experiments with a Vizard CAVE system. This software provided automatic data storage (i.e., logging the position of the observer and static/dynamic elements) and logic units to setup the experiment. The obtained data was stored in a MySQL database (version 5.6.16).

In this experiment, one virtual environment was used for two different spatial navigation tasks. This environment consisted of a small meadow (40 meters x 40 meters) with randomly placed spheres. Each sphere had a radius of 0.25 meters, floated 0.25 meters above ground, and had a minimum distance of 2 meters to the nearest sphere.

3.1.3 Procedure

Participants first completed a joystick training task to familiarise with the virtual environment and the joystick. In this phase, participants were asked to use the joystick to move around and collect (using the "catchment" area) 10 of 40 randomly coloured and placed spheres.

Next, participants were trained in five trials in two different tasks (i.e., response and place learning tasks) with respective navigation aids. Following the training trials in each task, participants were tested without any navigation aid in a test trial.

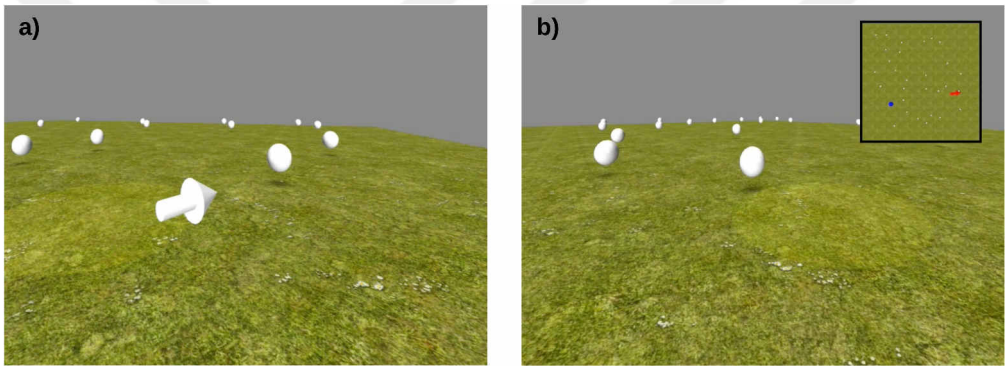

Figure 8: (a) The virtual environment used in the response learning task where participants were trained to follow a route with the help of an arrow and then reproduce the route without the arrow. **(b)** Virtual environment for place learning task where participants were trained to move from a starting location indicated with a red arrow on the map to a goal indicated with a blue dot on the map and then required to reproduce without the map.

In response learning task (referred also as compass task; screenshot given in Figure 8a) participants were trained in five trials to reach a blue target sphere by following a fixed route indicated by an arrow. In the test trial, participants were required to reproduce the same route without the arrow. In this task, seven behavioral scores were measured for each participants which are described below.

compass 1, 2, 3, 4, 5: Time required for the participant to reach the target sphere in each of the five training trials of the compass task, respectively (unit: seconds).

compass test: Time required for the participant to reach the target sphere in the test trial of the compass task. (unit: seconds)

compass slope: Behavioral score that is calculated from the slope of a line fitted to training trial scores of compass task as a measure of response learning.

In place learning task (referred also as map task; screenshot given in Figure 8b) participants were trained in five trials to reach a blue target sphere using a map. This map showed the location of the target and the starting points and the facing directions of the participants. Participants were then required to reach the target without using the map. Similar to the compass task, seven behavioral scores were measured for each participant. Below are the descriptions of these measures.

map 1, 2, 3, 4, 5: Time required for the participant to reach the target sphere in each of the five training trials of the map task, respectively (unit: seconds).

map test: Time required for the participant to reach the target sphere in the test trial of the map task. (unit: seconds)

map slope: Behavioral score that is calculated from the slope of a line fitted to training trial scores of map task as a measure of place learning.

3.2 Image Preprocessing

MRI scans of participants were performed with a 3.0-T MR 750 scanner (General Electric Medical Systems, Milwaukee, WI, USA). High-resolution 3D T1-weighted images were acquired with a spoiled gradient echo (SPGR) scan (TR, 9.94 ms; TI, 600 ms; FOV, 25.619.2 mm; matrix, 256192; flip angle 8; axial plane; slice thickness, 1 mm; 172 slices).

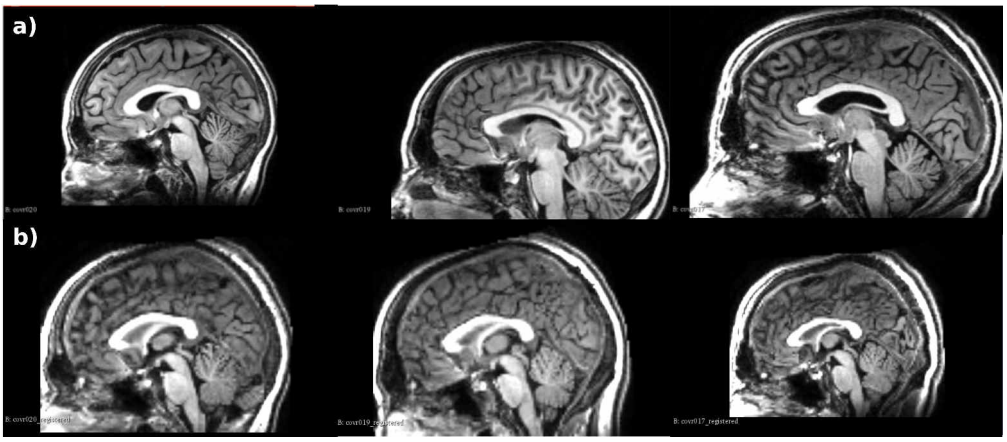

Figure 9: (a) Anatomical brain images of subjects number 20, 19 and 17, sagitally displayed with Slicer 3D software. The brains are completely misaligned due to anatomical differences in shape and size. **(b)** Anatomical brain images of subjects number 20, 19 and 17, sagitally displayed with Slicer 3D software. The misalignment problems due to size and shape differences are corrected.

Given the large anatomical differences found in original scans, images were preprocessed before any further analysis was conducted (Figure 9a). We used the Oxford Centre for Functional Imaging of the Brain (FMRIB)'s Software Library (FSL) for all preprocessing steps (Smith et al., 2004; Woolrich et al., 2009; Jenkinson et al., 2012). First, the brain tissues in the images were extracted using FSL Brain Extraction Tool (FSL BET; Smith, 2002) to Gray Matter (GM), White Matter (WM) and Cerebrospinal Fluid (CSF). Then, FSL Linear Image Registration Tool (FLIRT; Jenkinson and Smith, 2001; Jenkinson et al., 2002) was utilized to find affine transformations and to linearly register images into MNI152 standard space. After that, non-linear transformation to warp the brains into MNI152 standard space was calculated using FSL Non-linear Image Registration Tool (FNIRT) and then applied (Figure 9b).

The final step of the preprocessing was the bilateral segmentation of the hippocampus and the caudate from the aligned structural images of participants (Figure 10). We used FSL FIRST in order to segment each subject's hippocampus and caudate, a fully automated Bayesian segmentation that utilizes 336 manually labelled T1-weighted MR images with 15 different subcortical structures as training information (Patenaude et al., 2011).

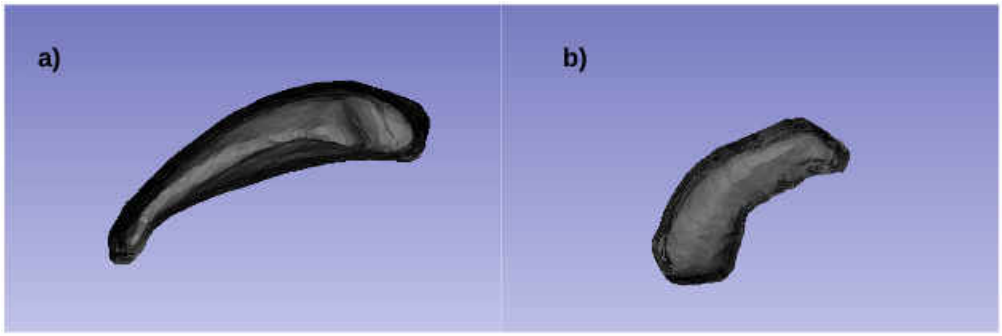

Figure 10: Aligned and segmented **(a)** the left caudates and **(b)** the left hipocampi of all participants shown on Slicer 3D software. Similarly, the right caudates and hippocampi of the participants were also segmented after alignment.

3.3 SPHARM Decomposition

In this work, we used SPHARM in order to extract the local features from the segmented hippocampi and caudates. SPHARM decomposition is a procedure for the explicit parametric representation and global description of simply connected 3D objects (Brechbühler et al., 1995). It is best understood as the 3D analogous of the 2D Fourier series representation of signals. Each individual SPHARM description is composed of a set of coefficients weighting the basis functions, (i.e., the spherical harmonics). Indeed, Szekely et al. (1996) have demonstrated that the SPHARM descriptions can be used to express local shape deformations (Szekely et al., 1996). For this reason, SPHARM decomposition was chosen to investigate the local shape changes in the hippocampus and the caudate due to navigation tasks.

3.3.1 Mathematical Description of SPHARM Decomposition

Brechbühler et al. (1995) described the SPHARM decomposition procedure with the following steps. First, the 3D structure was represented as surface meshes. Then, using the surface mesh representation, spherical parametrization that maps the surface of the 3D structure to a unit sphere was computed. In other words, one-to-one mapping between each point on the 3D surface $\vec{v}(\theta,\phi) = (x(\theta,\phi), y(\theta,\phi), z(\theta,\phi))^T$ and each point on the unit sphere was calculated following Eq. (1).

$$\vec{v}(\theta,\phi) = \sum_{l=0}^{\infty} \sum_{m=-l}^{l} \vec{c}_l^m Y_l^m(\theta,\phi) \tag{1}$$

where the coefficients $\vec{c}_l^m$ (i.e, SPHARM coefficients) are 3D vectors due to the three different coordinates and $Y_l^m(\theta, \phi)$ are spherical harmonics of degree l and order m, defined on $\theta \in [0, \pi)$ and $\phi \in [0, 2\pi)$. Spherical harmonics are mathematically described with the Eq. (2) given below.

$$Y_l^m(\theta, \phi) = \sqrt{\frac{2l+1}{4\pi} \frac{(l-m)!}{(l+m)!}} P_l^m(cos(\theta)) e^{im\phi} \tag{2}$$

where $P_l^m(w)$ are the associated Legendre polynomials defined as in Eq. (3).

$$P_l^m(w) = \frac{(-1)^m}{2^l l!} (1-w^2)^{\frac{m}{2}} \frac{d^{m+1}}{dw^{m+1}} (w^2-1)^l \tag{3}$$

Spherical harmonics with degree $l = 1, 2, 3, 4$ and order $m = 0, \ldots, l$ obtained with MATLAB are shown in Figure 11. Only the spherical harmonics with positive orders are shown because spherical harmonics with negative orders are symmetric to those with positive orders.

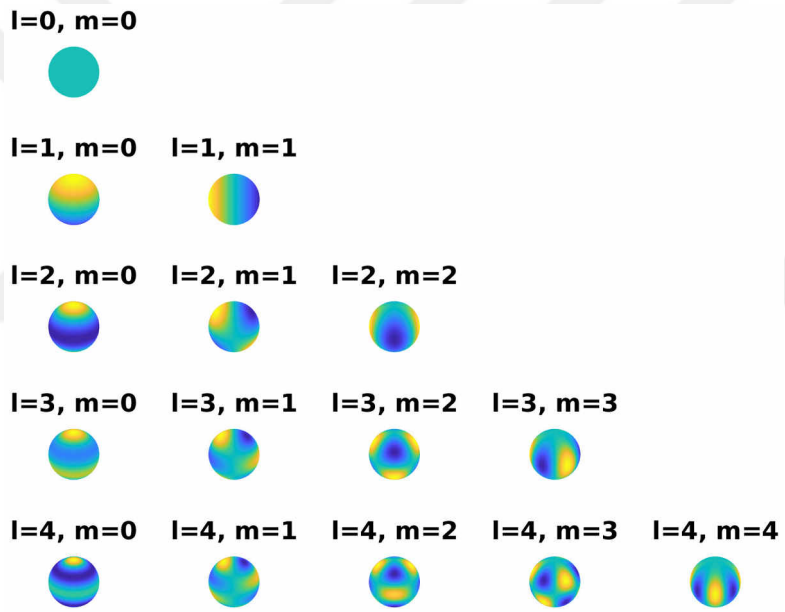

Figure 11: Spherical harmonics with degree zero to four and all possible positive orders thereof. The regions shown in yellow show inflation of the sphere normal to the surface and blue regions show deflation normal to the surface. Linear combination of spherical harmonics weighted with the respective coefficients yields an approximation of the original surface and each individual spherical harmonic depicts a local shape change multiplied with its weight.

3.3.2 SPHARM-PDM Pipeline

In order to obtain SPHARM coefficients, we used Slicer 3D software (developed by University of North Carolina and the National Alliance for Medical Imaging Computing, version 4.8; Slicer.org, 2018; Fedorov et al., 2012). The process of obtaining SPHARM coefficients and the reconstructed images from SPHARM-PDM involved three main stages.

In the preprocessing stage, holes in the segmented binary images were filled and spherical topology was ensured by applying two smoothing operations before SPHARM decomposition (Brechbühler et al., 1995).

In the second stage, input image (i.e., the binary segmentation) was first converted to surface meshes (Figure 12a). Then, pointwise mapping of the surface to unit sphere was calculated. To that end, a spherical mapping that followed two main properties was employed to ensure homogenous distribution of the parameter space for an efficient decomposition of the surface into SPHARM representation (Brechbühler et al., 1995). First, the mapping was area preserving meaning that every object region mapped to a region of proportional area in parameter space. Spherical mapping was also distortion minimizing meaning that every quadrilateral in object space was mapped to a spherical quadrilateral in parameter space (Styner et al., 2006). The spherical parametrization of the surface mesh can be observed in Figure 12b.

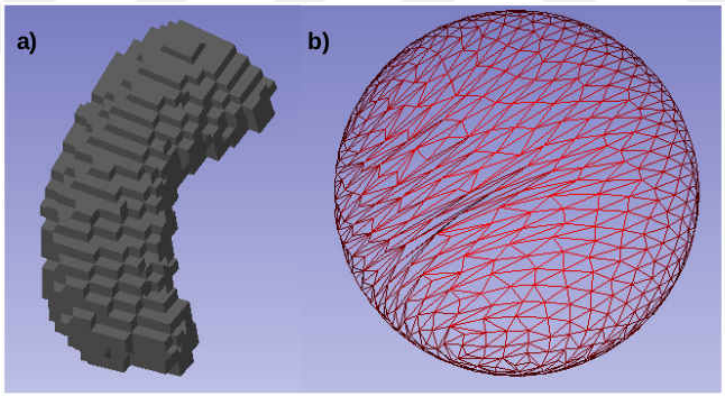

Figure 12: **(a)** Surface mesh representation of an example subject's left hippocampus. The surface appears block due to marching cubes algorithm (Lorensen and Cline, 1987). **(b)** Calculated spherical parametrization shown on unit sphere. Area preserving, distortion minimizing spherical mapping is used to ensure efficient decomposition of the surface to SPHARM coefficients.

The final step involves the calculation of SPHARM coefficients, calculation of SPHARM-PDM representations and reconstruction of images using the SPHARM-PDM representations. Here, first two orders of SPHARM coefficients were estimated from the surface mesh (and its spherical parametrization) utilizing least-squares optimization (Gutman et al., 2009)[1]. These coefficients were used to reconstruct first-order ellipsoids for all subjects and these ellipsoids were aligned to match the center and the first axes for normalization purposes (Gerig et al., 2001). Following the first-order ellipsoid alignment, SPHARM coefficients were extracted up to a user-defined SPHARM degree of l. The SPHARM degree controls the level of details and higher degree results in finer details on the reconstructed image (Figure 13a). In this study SPHARM degree was chosen as 20 since it provides acceptable degree of smoothing for the subcortical structures under investigation (Gerardin et al., 2009).

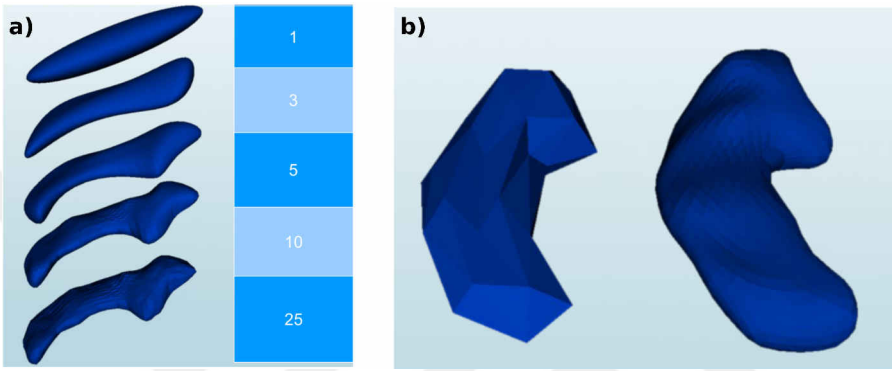

Figure 13: Effects of user-defined parameters in SPHARM-PDM reconstruction (adapted from Pascal et al., 2017) **(a)** Illustration of the effect of SPHARM degree as shown on a lateral ventricle. The SPHARM-PDM reconstructed image becomes more and more detailed as the level of SPHARM coefficient degree is increased. **(b)** The effect of icosahedron subdivision value on SPHARM-PDM reconstruction shown on hippocampus. The image on the left was reconstructed with subdivision level 2 and consists of only 42 vertices, whereas the image on the right was reconstructed with subdivision level 10 and consists of 1002 vertices. The hippocampus on the right is seen to have much higher degree of smoothness.

SPHARM description of the surface was then sampled into triangulated surfaces via icosahedron subdivision (Styner et al., 2006). The main parameter that controlled the icosahedron subdivision was the subdivision level which determined the number of vertices in the SPHARM-PDM reconstructed images. Consequently, the icosahedron subdivision level value controlled the smoothness of the reconstructed images (Figure 13b).

[1]Before any shape analysis is carried out, shapes have to be normalized with respect to a coordinate frame.

The smoothness of the SPHARM-PDM reconstructed images were critical in this work since a locally detailed statistical analysis was necessary to accurately describe local changes in the hippocampus and the caudate. Therefore, we employed a subdivision level value of 20 resulting in 4002 vertexes. Figure 14 presents a icosahedron subdivision of the left hippocampus for a participant in the experiment. This subdivision represents the parametrization on a unit sphere for SPHARM-PDM representation of the original object. From the icosahedron parametrization via reverse spherical mapping (Eq. (1)) SPHARM-PDM reconstructed images are calculated. These reconstructions played an essential role both in cross-checking the accuracy of SPHARM coefficients' ability to represent the original object and in carrying out statistical shape analysis.

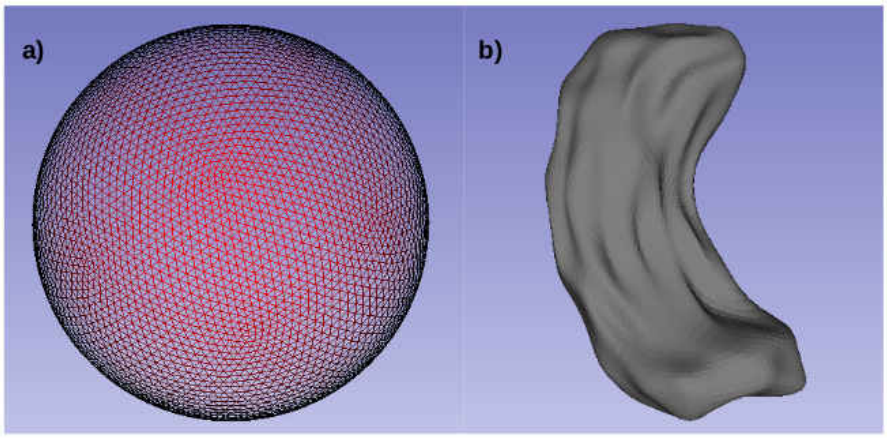

Figure 14: Icosahedron subdivision and following SPHARM-PDM reconstruction obtained from SPHARM coefficients of an example participant's left hippocampus **(a)** The unit sphere parametrization from icosahedron subdivision using subdivision level value of 20. **(b)** SPHARM-PDM reconstruction of left hippocampus following the icosahedron subdivision.

In this study, each lateral subcortical structure of each subject is represented by 1323 SPHARM coefficients following a SPHARM decomposition of degree 20 since each dimension is represented by $(20+1)^2 = 441$ and SPHARM coefficients of three dimensions are concatenated, resulting in $441 \cdot 3 = 1323$ features for each structure.

3.4 Classification

In order to utilize the local features of the subcortical structures to predict the spatial navigation abilities, a classification algorithm needs to be trained. There are various classification algorithms with different advantages and drawbacks. Support Vector Machines (SVM) is a supervised algorithm that lies at the intersection of learning theory and practice. Success of SVM in AD studies, which is in close relation with spatial navigation, has been proven in previous works of Gerardin et al., 2009, Gutman et al., 2009, Li et al., 2007. One main drawback of SVM is that while it is a powerful binary classifier, it is yet to be developed to perform multi-class classification (Hsu and Lin, 2002). However, since this study deals with good and bad navigators depending on their performances, binary classification is sufficient.

In addition, in order to account for the drawback of having twenty data points (participants in the VR study) in the dataset, two-nested CV algorithm is integrated into SVM classification to avoid overfitting. Overfitting is a known issue in machine learning and classification in which the dimensionality of the feature space is large (1323 in this case) and the number of the data is very small in comparison (20 in this case). In such situations, it is possible to find a decision function that separates the training data but may not generalize well to unseen data (Guyon et al., 2002). After accounting for overfitting, the accuracy of prediction further enhanced with a feature ranking algorithm of SVM-RFE and a following feature selection.

3.4.1 Support Vector Machines (SVM)

SVM is a novel supervised learning algorithm which tries to fit a hyperplane with maximum margin in a multidimensional feature space (or transformed feature space) that splits the training data while maximizing the distance of nearest cleanly split training data to the hyperplane (Maimon and Rokach, 2010; Cortes and Vapnik, 1995, Figure 15).

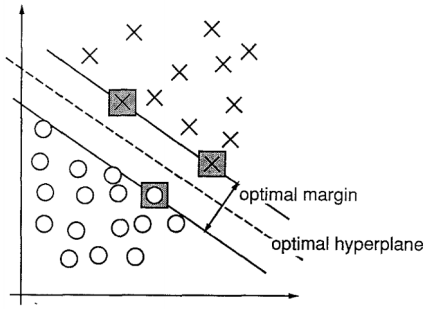

Figure 15: Basic illustration of SVM for a classification with 2D feature space (Cortes and Vapnik, 1995). SVM tries to find an optimal hyperplane that separates two classes from each other. In addition, the support vectors (i.e. the vectors on the boundary of the margin from each class) is also shown with gray squares.

While the detailed mathematical foundations of SVM is given in Appendix A, it is also briefly discussed here to provide basis for subsequent chapters. The optimal hyperplane in SVM requires margin to be maximum and no data point to lie inside the margin. Therefore, following equations construct the optimization problem to be solved in d-dimensional SVM problem;

$$max_{\vec{w}\in\Re^d, b\in\Re} \frac{2}{||\vec{w}||} \quad \text{or} \quad min_{\vec{w}\in\Re^d, b\in\Re} \frac{1}{2}||\vec{w}||^2, \qquad \text{maximization of the margin} \tag{4a}$$

$$\text{subject to} \quad y_i(<\vec{w}, \vec{x_i}> +b) \geq 1, \forall i \in 1, \ldots, n, \qquad \text{no data inside margin} \tag{4b}$$

where $\vec{w}$ is the normal vector to the hyperplane, b is the offset, $\vec{x_i}$ are the training data points, the y_i are the respective labels and n is the total number of data. Once the parameters $\vec{w}$ and b is found, unseen data, $\vec{x}$, can be classified using the decision function given in Eq. (5).

$$f(\vec{x}) = sgn(<\vec{w}, \vec{x}> +b) \tag{5}$$

One advantage of SVM is that since the decision is simply made based on an inner product, SVM can be extended to different data structures and feature spaces through kernelized-SVM (Adamiak et. al, 2016). A kernel is defined as an inner product in a transformed feature space with a transformation (Eq. (6))

$$\kappa(\vec{x_1}, \vec{x_2}) =< \phi(\vec{x_1}), \phi(\vec{x_2}) > \tag{6}$$

where ϕ is an arbitrary transform. Kernelization reduces the computational complexity of transforming the data and the support vectors to a feature space since well-defined kernels can directly be applied to the vectors to calculate the inner product in a transformed feature space. This allows not only the extension of SVM to complex data structures such as strings and graphs, but also the computation of inner products in a more complex feature space for vector data. Gerardin and colleagues (2009) carried out classification analysis on AD patients with linear and Radial Basis Function (RBF). They demonstrated that the RBF kernel was better at separating the local features of the hippocampus than the linear kernel (Gerardin et al., 2009). For this reason, RBF kernel (Eq. (7a)) was used for the classification in this study but linear kernel (Eq. (7b)) was also necessary for SVM-RFE feature selection.

$$\kappa_{RBF}(\vec{x_1}, \vec{x_2}) = e^{-\frac{1}{2\sigma^2}||\vec{x_1}-\vec{x_2}||^2} \quad \text{RBF Kernel} \tag{7a}$$

$$\kappa_{linear}(\vec{x_1}, \vec{x_2}) =< \vec{x_1}, \vec{x_2} > \quad \text{Linear Kernel} \tag{7b}$$

One final modification to the SVM defined with the conditions given in Eq. (4) is necessary to enhance the practicality of the algorithm. Those conditions of the so-called Hard-Margin SVM does not allow any training data to be placed inside the margin defined by the support vectors. However, the data may not be completely separable and such optimal hyperplane may never be found depending on the dataset. Indeed, previous research on AD has shown that the data points described with local features of the hippocampus are not completely separable (Li et al., 2007; Gerardin et al., 2009). Therefore, Soft Margin C-SVM proposed by Cortes and Vapnik (1995) is used in this study where the training data is allowed to be inside the margin but is punished with an error variable (ξ_i, Eq. (8b)) depending on its proximity to its own class boundary.

$$min_{\vec{w}\in\Re^d, b\in\Re}\frac{1}{2}||\vec{w}||^2 + C\sum_{i=1}^{n}\xi_i \quad \text{subject to} \quad y_i(<\vec{w}, \vec{x_i}> +b) \geq 1-\xi_i, \forall i \in 1, \ldots, n \tag{8}$$

3.4.2 Two-Nested Cross Validation (CV)

In machine learning, different algorithms need to be compared with each other and the most common performance evaluation is the accuracy check on an unseen test set with known class labels after the model is determined using the training data. This distinction between the test and training data sets is important because if the test set is included in the training set, the accuracy result may be biased and may not generalize well to unseen dataset. This phenomenon

is known as overfitting and it must be avoided by separating the test set to yield a reasonable comparison between different algorithms. Although various separations of the entire dataset into train and test sets are possible, the most common one is the 80-20 split where 80% is separated for training and 20% is separated for test set (Agranoff et al., 2006; Crowther and Cox, 2005; Liu et al., 2014, flowchart given in Appendix B).

When the dataset is small and it is not possible to split the data into train-test sets, it is conventional to use k-fold CV for training (Stone, 1974). In k-fold CV, the dataset is split into k different folds and each fold is used as test set. Then, the accuracy measure is repeated for every fold. The performance evaluation is based on the average accuracy over all possible train-test combinations (for flowchart see Appendix B).

In addition to performance evaluation, there are number of user-defined parameters that need to be selected which can optimize the performance for every classification algorithm. This optimization procedure is called the model selection and lies at the heart of most classification problems (Cawley and Talbot, 2010). In this work C-SVM classification with RBF kernel was used which introduced two optimization parameters, C and γ. Parameter C controls the trade-off between the error introduced by allowing data points inside the margin and the margin size. Parameter γ is a transformed variable ($\gamma = -\frac{1}{2\sigma^2}$) that controls the variance of the RBF kernel.

The search for all possible hyperparameters is practically impossible since there are infinitely possible values. Therefore, a conventional and sufficient way for model selection is to reduce the search to a finite subset of hyper-parameters with iterative algorithms and try to find a local optimum instead of searching all possible values of hyper-parameters (Keerthi, 2002). One strategy that is commonly applied in model selection is called grid search (Lerman, 1980; Kavzoglu and Colkesen, 2009). In the grid search algorithm, first the finite subset for possible hyper-parameter values are determined. Then, all possible models constructed with all possible combinations of hyper-parameters are checked. Finally, the model yielding the best accuracy is selected. Computationally, grid search algorithm is applied with n-nested for loops where n is the number of hyper-parameters in the search. In this study, there were two different hyperparameters that needed to be tuned which yielded a two-nested for loop (C in range $2^0, 2^1, \ldots, 2^{20}$ and γ in range $2^{-15}, 2^{-14}, \ldots, 2^0$).

The data used to train the models with different parameter combinations should clearly be separated from the dataset on which the accuracy scores are tested as it also results in overfitting similar to performance evaluation. Therefore, the general approach is to split the dataset apart from the test set into validation and training sets. Then, the models with different hyperparameter combinations are constructed using the training sets and the best model is selected based on the prediction accuracy on the validation set. Overall, this approach requires the dataset to be divided into three separate sets. In brief, the training set is used to construct various models with different combinations of hyperparameters and the validation set is utilized in the evaluation and selection of models. Finally the test set, which is kept away from all computation, is used for unbiased evaluation (for flowchart see Appendix B).

The problem of having a small dataset becomes more significant when model selection and performance evaluation needs to be combined since this small dataset needs to be separated into three different datasets. In order to get unbiased performance evaluation the proposed algorithm in this work is the two-nested CV. This algorithm has been shown to reduce the bias considerably and give an estimate accuracy very close to that obtained on an independent dataset (Varma and Simon, 2006). In this algorithm, CV is employed both in the model selection and the performance evaluation, resulting in a two nested loops. Within the outer loop (i.e, performance evaluation loop), a fold is completely separated as test set and the remaining folds are passed onto inner loop (i.e, model selection loop). In the inner loop, performance of every hyperparameter combination is evaluated on validation sets using k-1-fold CV and the validation test is rotated among the remaining folds after the test set is separated. The inner loop passes the best parameter combination to the outer loop where the fitted model is tested on a completely isolated test fold. Finally test folds are rotated in k-fold CV and calculated accuracies are averaged to report as an indicator of how well the subcortical structure can predict a given behavioral test (Figure 16).

3.4.3 Feature Selection

Feature selection is an integral part of every machine learning algorithm since redundant, noisy data of little or no discriminatory power degrades the performance of a decision function and reduces the accuracy of prediction (Ambroise and McLahlan, 2002; Huang et al., 2014). In

biomedical machine learning problems, the significance of feature selection becomes much more prominent since in most applications there are only few data as compared to huge amount of features (Guyon et al., 2002). In this study a similar situation was present. There was only data for twenty participants compared to over a thousand features coming from the SPHARM coefficients. Furthermore, each of these coefficients describes a mode of deformation and feature selection was necessary to correctly describe local shape changes in the cortical structures. Therefore, a suitable feature selection algorithm was required to enhance the performance of classifier accuracy.

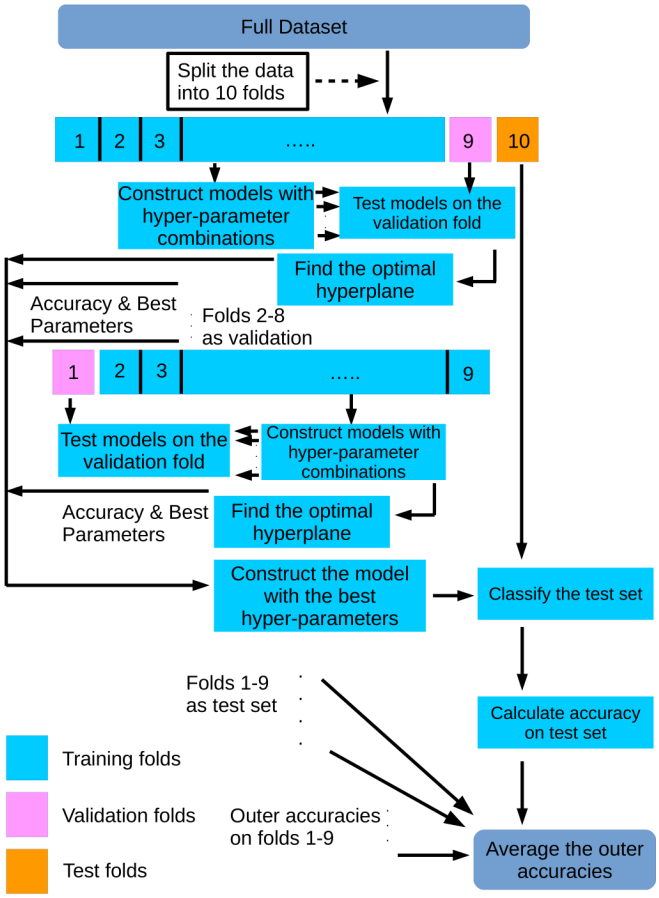

Figure 16: The flowchart of two-nested 10-fold cross validation for model selection and performance evaluation in SVM classification. Training folds are shown with cyan, validation folds are shown with magenta and test folds are shown with orange. In each outer loop one fold is fixed and separated as test fold while the other folds are used in 9-fold CV to determine best model using grid search algorithm. Performance of one outer loop is then tested with the best model on the separated test set. Overall performance evaluation is given by the average accuracies obtained from all test folds in the outer k-fold CV.

Feature selection methods are categorized into filter methods, wrapper methods and embedded methods (Saeys et al., 2007). Filter methods rank the features solely looking at the intrinsic properties of the data completely disregarding the interaction with the classifier. Wrapper approaches select the relevant features for a given classifier by evaluating the performance of the classifier but are prone to overfitting more than filter methods. Embedded methods also integrate the classifier in the feature ranking but these methods are embedded in the classification algorithm itself and yield much less biased performance.

SVM-RFE is an embedded feature selection that was first proposed by Guyon et al. (2002). In this method, a SVM classifier with a linear kernel is trained and the features are ranked according to their weight magnitude in the trained SVM classifier. The feature with the least weight is eliminated from the features as the least relevant feature and the process is iterated until all features are ranked (Guyon et al., 2002). In this study, description of local changes in subcortical structures that was related to the behavioral tests was important. In addition, SVM was chosen as method of classification. For these reasons, SVM-RFE was selected as feature selection method since it integrates the intrinsic properties of SVM and information from behavioral tests into selecting relevant local descriptors.

A selection is made after all the features are ranked. There are two main methods for feature selection. The first category tries to locally optimize performance evaluation iteratively by adding the features from the top of the list one-by-one. Another category is a simple thresholding method where the researcher determines a specific number of features from the top of the ranked features list to be used in classification. In this study, a mixture between thresholding and local optimization was used in order to reduce the computational complexity. The features were selected from the ranked list with a fixed threshold but the performance of the classifier was monitored for variety of threshold values (Gerardin et al., 2009). The performance of the classifier was observed both in full range of features from 1 to 1323 with steps of 43 and also with a feature resolution of 1 around the number of features which yielded maximum accuracy.

Although the advantages of feature selection are numerous and it is necessary to include in most machine learning applications, the data used in the feature selection must be chosen carefully in embedded feature ranking algorithms since the classifier used in feature selection is

also used in the performance evaluation. As such, the use of the test data in feature ranking and selection may result in a selection bias (Ambroise and McLahlan, 2002). In this study the feature ranking method was an embedded method and was carefully incorporated into two-nested CV algorithm. SVM-RFE was integrated inside the outer loop and repeated whenever the test data is rotated in the cross validation. Therefore, the test folds were never used for the SVM-RFE ranking. Although the re-applying feature selection inside the outer loop is an additional computational effort, it was done in order to avoid selection bias.

3.5 Statistical Analysis

The primary goal of statistical analysis was to observe localized shape changes in subcortical structures that provided discriminative power for high prediction accuracies. In addition, statistical analysis also provided insight into whether the correlations that yielded high accuracy results are positive or negative since negative correlation also yields high predictive power (anti-learning). To that end, two methods were employed to show statistical significance. First, the VBM was used with behavioral tests that were predicted with high accuracy in order to see the significantly correlated regions across whole brain. However, the VBM is not sensitive enough to provide details regarding the local shape changes on structures. Therefore, local statistical shape analysis was carried out using the SPHARM-PDM reconstructed images in order to localize significantly correlated regions on the structures and demonstrate the direction of the change (whether it is an inflation or deflation).

3.5.1 Voxel Based Morphometry (VBM)

The VBM is a global method that uses the behavioral scores to show where the correlations lie in the overall brain depending on differences in gray matter volume. The VBM provides a statistical approach that requires no a priori information and carries out correlation analysis over all gray matter volume in the brain. While the VBM is useful in determining significantly correlated volume changes, it is a global approach that does not provide enough sensitivity to indicate local changes.

In this work, the VBM was applied with the behavioral test scores in the compass and the map tasks that were predicted with high accuracy in classification to see correlated regions across

whole brain. While the classification results were obtained by using local features of structures, the VBM was also included in the study to validate that these correlations coincided with structures that predicted that particular test with high accuracy. Furthermore, inclusion of the VBM allowed for the observation of the localization that can be achieved with global statistical analysis and provided a ground for comparison with local statistical analysis.

In order to show positive and negative correlations, two different General Linear Models (GLMs) are created for each of those behavioral test that was predicted with high accuracy. The scores were based on time required to complete the tasks and higher score showed worse performance. Similarly, learning slopes that are less negative showed a slower learning performance and thus indicated negative correlation. For this reason, GLM obtained with direct inclusion of the demeaned scores is utilized in the depiction of negative correlation. In order to show positive correlations, secondary GLMs are created where the signs of the scores are reversed.

After GLMs are created, structural data was analyzed with FSL-VBM (Good et al., 2001; Smith et al., 2004; Douaud et al., 2007). First, structural images were brain-extracted and gray matter-segmented before being registered to the MNI152 standard space using non-linear registration (Andersson et al., 2007). The resulting images were averaged and flipped along the x-axis to create a left-right symmetric, study-specific gray matter template. Second, all native gray matter images were non-linearly registered to this study-specific template and modulated to correct for local expansion (or contraction) due to the non-linear component of the spatial transformation. The modulated gray matter images were then smoothed with an isotropic Gaussian kernel with a sigma of 3 mm. Finally, voxelwise GLM created with the behavioral test scores was applied using permutation-based non-parametric testing, correcting for multiple comparisons across space.

3.5.2 Statistical Shape Analysis using SPHARM-PDM Reconstructed Images

In statistical analysis of anatomical structures, gross shape measures such as volume have been widely used. Paniagua et al. (2009) proposed a new method which can locally show statistical significances based on SPHARM-PDM reconstructed images (Paniagua et al., 2009). Indeed, Gerardin and colleagues (2009) have demonstrated locally significant atrophies on the hippocampus of AD patients using this method (Gerardin et al., 2009). As previous studies have shown

(Maguire et al., 2000; Schinazi et al., 2013), spatial navigation related volume changes are also substantially local rather than global. For these reasons, this method was chosen to provide higher sensitivity and more localized significant regions on structures compared to global statistical analyses such as the VBM.

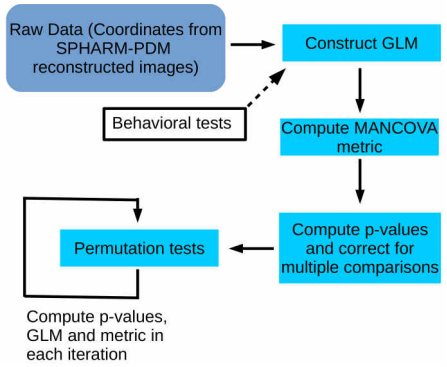

Figure 17: Flowchart of the Shape Analysis MANCOVA. Raw data from SPHARM-PDM reconstructed images were taken and combined with the behavioral tests to construct GLM. Next, multivariate statistics were calculated with a chosen metric. Based on this metric, significance (p) values are calculated and corrected for multiple comparisons using permutation tests.

The main tool used in the statistical shape analysis is the MANCOVA. The MANCOVA tool tests for differences between groups at every surface location in SPHARM-PDM reconstructed images (for workflow, Figure 17). In this approach, raw data (i.e, the vertices) from the SPHARM-PDM reconstructed images are taken and a general linear model with the behavioral test scores are constructed. Then, multivariate statistics of (x,y,z) locations is calculated with a modified Hotelling-metric (Equation 9)

$$T^2 = (\mu_1 - \mu_2)^T (\Sigma_1 \frac{1}{n_1} + \Sigma_2 \frac{1}{n_2})^{-1} (\mu_1 - \mu 2) \tag{9}$$

where μ, Σ stands for mean and covariance matrix, respectively and n stands for the number of the subjects in each group. Then, the significance of the T^2 metric is evaluated at each location via permutation test approach with a null hypothesis that the distributions of the locations at each spatial element is the same for every subject regardless of the group. Paniagua et al. (2009) also stated that permutation number from 20000 up should yield results that are negligibly different than using all permutations (Paniagua et al., 2009). Therefore, permutation number was also chosen as 20000 in this work.

In this study, local shape analysis using the MANCOVA involved testing a hypothesis per surface element. With an icosahedron division level of 20 this amounted to 4002 points in each SPHARM-PDM reconstructed images and thus correction for multiple comparison was also needed. There are two corrections applied in this study, namely Bonferroni correction to control for the Family Wise Error Rate (FWER) and False Discovery Rate (FDR) correction which controls the number of false positives in the vertex-wise hypothesis testing across the surface.

3.6 Complete Workflow

The objective of this Master's work was to locally investigate the hippocampus and the caudate with the behavioral scores from place and response learning tasks. To this end, MR images of the participants were aligned and their hippocampi and caudates were bilaterally segmented. Next, local shape descriptors (i.e, SPHARM coefficients) were extracted for each hippocampus and caudate. SPHARM decomposition was chosen as the shape analysis method because each SPHARM coefficient shows a mode of deformation and can be used to effectively indicate local shape changes. Then, these local descriptors were utilized as features in SVM classification to evaluate the correlation of structures with the behavioral tasks. However, due to a very small dataset size (number of participants, 20), two-nested CV (a very pessimistic training and testing algorithm) was used in order to reduce the intrinsic bias due to the dataset. In addition, feature selection using SVM-RFE algorithm was also included since accurate local description of shape changes were necessary.

Following classification, two different statistical analysis methods were carried out. First, the VBM is utilized with behavioral test that were predicted with high accuracy to observe whether these correlations aligned with the structures whose local features yielded high accuracy. However, the VBM is a global statistical analysis method that is not sensitive enough to show localized changes on structures. For this reason, a second and more local statistical analysis method that utilizes the reconstructed images from SPHARM coefficients was employed to provide higher degree of sensitivity and demonstrate better localization of significantly correlated regions.

The flowchart that summarizes the methodology used in this Master's study is given in Equation 18 below.

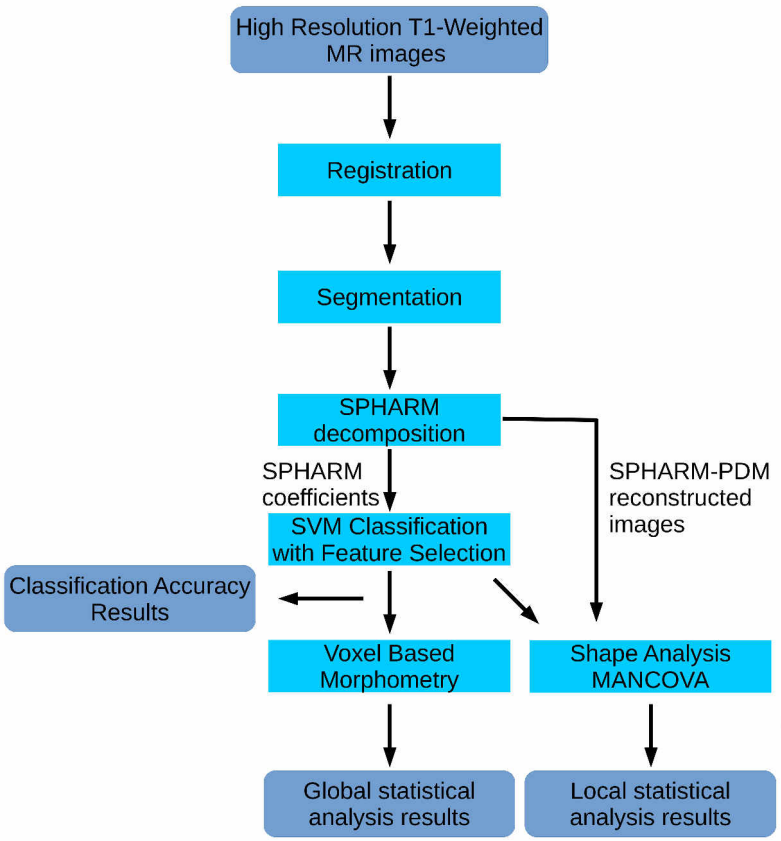

Figure 18: Overall flowchart of the methodology used in thesis work. MR images of participants were aligned and each participants' hippocampus and caudate were bilaterally segmented. Next, local shape descriptors from each structure were extracted using SPHARM decomposition. Then, SPHARM coefficients were used in SVM classification with two-nested CV algorithm incorporated with SVM-RFE feature selection. Finally, global and local statistical analyses were carried out using the VBM and the Shape Analysis MANCOVA methods.

4 Results

This chapter presents the results obtained in this study. The chapter begins with the description of the behavioral scores obtained during the VR experiment. Next, the prediction accuracies of the hippocampus and the caudate on behavioral tests are displayed with respect to the number of features. The structure-test combinations that yielded above 60% prediction accuracy are also presented around the peak accuracy value with a finer resolution. Following the classification results, global statistical analysis (i.e, the VBM) results are shown for the behavioral tests that were predicted with accuracy above 60%. Finally, local significance maps from the MANCOVA are displayed for structure-test combinations that showed more than 60% prediction accuracy.

4.1 Behavioral Data

During the experiment, the time required by participants to reach the target in training and test trials for both the compass and the map tasks were recorded in seconds. In addition, a line fitted to scores obtained during training sessions and its slope was calculated as a measure of learning in both tasks. The mean and the standard deviations of these scores were then calculated and no outliers were detected (Table 1, see Appendix C for complete table of scores).

	Training 1		**Training 2**		**Training 3**		**Training 4**		**Training 5**		**Test**		**Slope**	
	M	SD	M	SD	M	SD	M	SD	M	SD	M	SD	M	SD
Compass	45.44	18.74	44.65	18.37	41.40	15.48	40.67	14.16	39.51	15.82	46.16	15.52	-1.56	1.89
Map	82.75	47.34	52.59	42.12	35.65	31.64	27.05	22.45	23.70	19.43	19.79	7.26	-14.36	9.64

Table 1: Mean (M) and Standard Deviations (SD) of the behavioral scores obtained during the training and test sessions and calculated slopes from training data for both the arrow and the map task.

Inspection of the training session scores shows that participants were faster to complete the training trials of the compass task compared to the map task. However, participants' improvement over the trials was significantly better in the map task. This can be observed from the learning slopes of the map task. This improvement was also apparent during the test session in the map task. However, participants displayed worse performance in the arrow task test session compared to the training trials.

4.2 Classification Results

The prediction accuracies were obtained in the two-nested CV based SVM that utilizes the SPHARM coefficients (i.e., local shape descriptors) as features. In the preliminary analyses, the correlations between the hippocampus and the caudate and the behavioral scores in both tasks from initial training session, test trial and the slopes were evaluated using the prediction accuracies. To that end, the feature range was divided with equally spaced thirty-two points and the prediction accuracy was evaluated with the number of features at each point. The significantly correlated structure test combinations were determined from the maximum accuracies (Table 2).

According to these preliminary results, structures that predicted behavioral scores with strictly over 60% accuracy were regarded as significantly correlated with those behavioral scores. The prediction accuracies indicated that the left hippocampus was significantly correlated with the learning slope of the map and compass tasks. In addition, the right caudate was shown to significantly correlate with the map task test scores. The accuracy results also demonstrated that the right hippocampus was significantly correlated with the learning slope in the compass task and first training trial scores in the map task. While the left caudate achieved 60% predictability on the learning slope in the compass test, it was not considered significant.

	compass1	**compass slope**	**compass test**	**map 1**	**map slope**	**map test**
Left Caudate	30.31%	60%	39.06%	24.69%	25.63%	59.38%
Left Hippocampus	42.5 %	68.75 %	36.88%	42.5%	67.5%	47.81
Right Caudate	35.31%	45.94%	35.63%	51.88%	54.06%	67.81%
Right Hippocampus	53.13%	67.19%	28.44%	63.13%	40.94%	40.94%

Table 2: Prediction accuracies of structures on six different behavioral tests. The prediction accuracies that exceeded 60% were regarded as correlated structure test combinations in the study.

The preliminary accuracy results were also obtained for each one of the thirty-two equally spaced points and plotted against the number of features (see Figure 19 for significantly correlated combinations, see Appendix D for the rest). Inspection of these results, revealed an expected decrease in the accuracy with an increase in the number of features included in the classification. Furthermore, the peak accuracy was observed to occur with different number of features for each combination. While the peak accuracy was observed with smaller numbers of features for the map task scores, the maximum prediction accuracies occurred with large numbers of features for the compass task scores.

The initial accuracy results were obtained with a coarse resolution ($\sim$43 features) and showed the prediction accuracies for thirty-two different numbers of features. Although the initial coarse results indicated the correlated structure test combinations, further analysis with a finer resolution was carried out to identify the absolute peak accuracies. To that end, the structures that predicted map task scores with high accuracy were investigated with a single feature resolution in the feature range 1-50. The structures that were correlated with the compass task scores were investigated around the observed peak number of features also with single feature resolution.

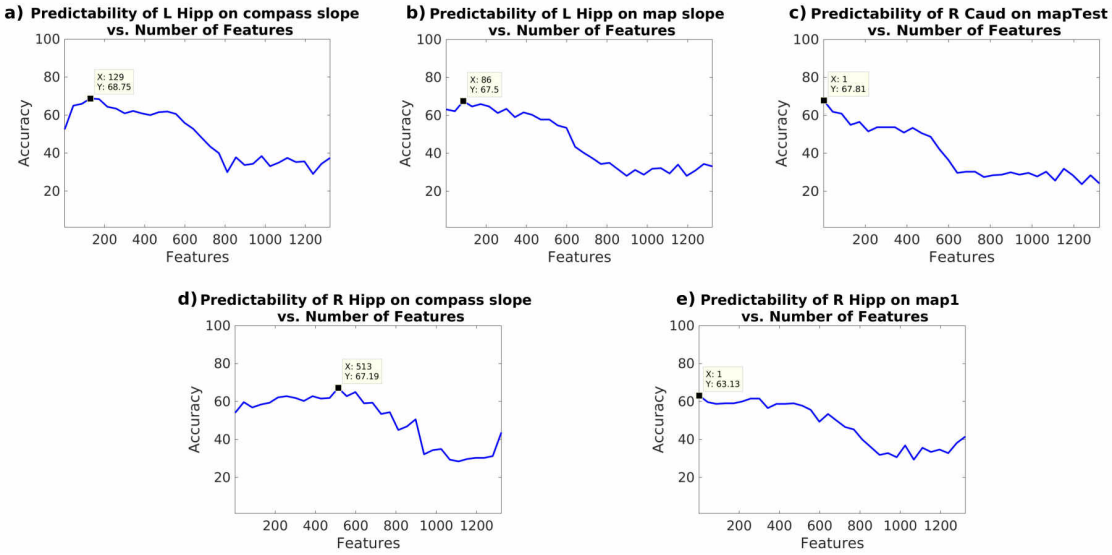

Figure 19: Prediction accuracies for significantly correlated structure test combinations plotted against number of features. In all plots the prediction accuracy was observed to decrease with increased number of features. The number of features that yielded maximum accuracy was small for the map task scores (smaller than 100; b,c,e) and larger for the compass task scores (larger than 100; a,d).

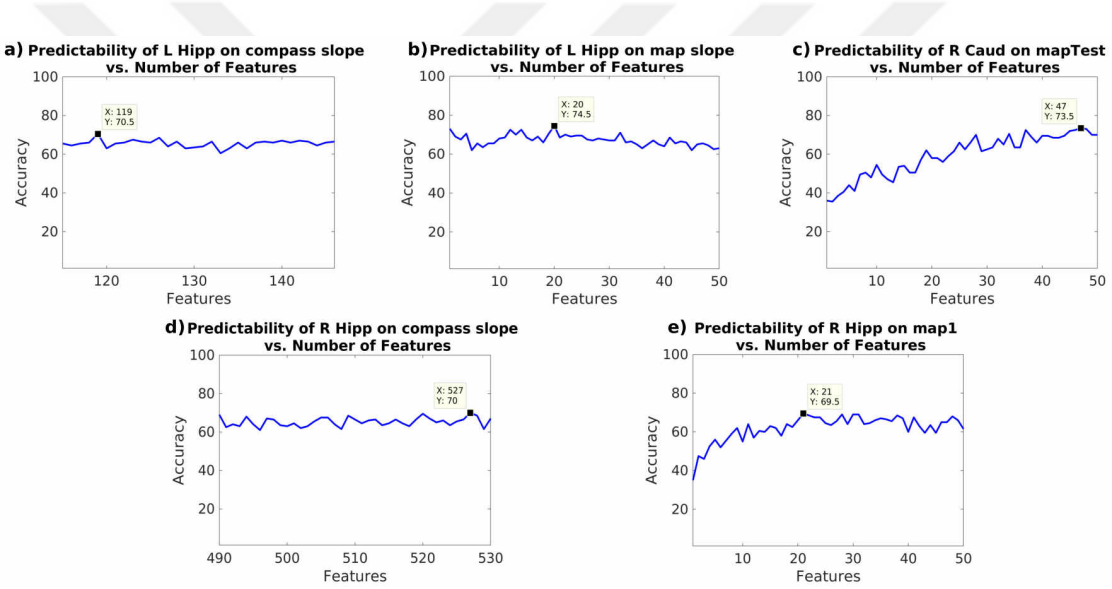

Figure 20: Detailed accuracy analysis for the five most correlated structure test combinations around the feature number where peak accuracy is observed with a single feature resolution. **(a)** Left hippocampus predicting learning slopes in compass task with 70.5% accuracy with 119 features. **(b)** Left hippocampus predicting learning slopes in map task with 74.5% accuracy with 20 features. **(c)** Right caudate predicting test scores in map task with 73.5% with 47 features. **(d)** Right hippocampus predicting learning slopes in the compass task with 70% accuracy with 527 features. **(e)** Right hippocampus predicting initial training scores in the map task with 69.5% accuracy with 21 features.

This fine resolution accuracy analysis demonstrated that the prediction of the left hippocampus on map slope increased to 74.5% at 20 features (Figure 20a) and on compass slope to 70.5% at 119 features (Figure 20b). The absolute peak accuracy between the right caudate and the map task test scores was found to be 73.5% with 47 features (Figure 20c). The absolute maximum prediction accuracy of the right hippocampus on the compass slope was observed at 527 features with 70% (Figure 20d) and on the first training trial scores of map task was observed at 21 features with 69.5% accuracy (Figure 20e).

4.3 VBM Results

Global statistical analysis with the VBM was carried out in order to show the volume changes that correlated with the behavioral tasks. To that end, behavioral scores that were predicted with high prediction accuracy (i.e., compass slope, map 1, map slope and map test) were used in the VBM to show both the positively and negatively correlated volume changes in the overall brain. Here a positive correlation (obtained with sign reversed scores since higher time scores meant lower performance) indicates larger gray matter volume. In contrast a negative correlation indicates less gray matter volume. Only the uncorrected p-value maps are shown since the statistical significances did not survive the correction for multiple comparisons.

4.3.1 Left Hippocampus

Classification results revealed that the left hippocampus predicted learning slopes in the map and compass tasks with 74.5% and 70.5% accuracy, respectively. The VBM analysis with map slope scores showed a positive correlation around the tail region of this structure and a negative correlation around the body and the head regions (Figure 21a). According to these results, participants that displayed better improvement over map task training trials had larger gray matter volume in the tail region and less gray matter volume in the body and the head regions. On the other hand, the VBM results with compass slope scores revealed a positive correlation in the head of the left hippocampus and a negative correlation in the body of the left hippocampus (Figure 21b). These results indicate that the participants with higher compass slope scores had larger gray matter volume in the head region and less gray matter volume in the body region.

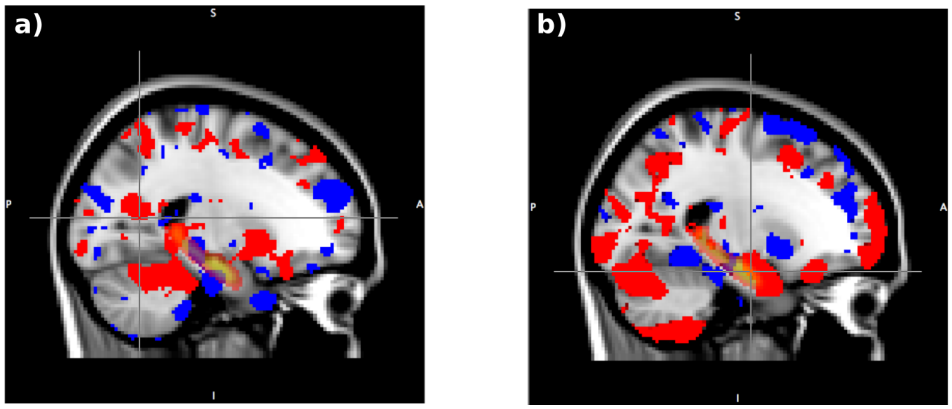

Figure 21: The VBM results (sagittal view) showing the positively (red) and negatively (blue) correlated volume changes shown on the left hippocampus (red-yellow) which was localized with Harvard subcortical structures atlas. **(a)** Correlation with map slope scores. Positive correlation (increased volume) is observed in the tail region and negative correlation (decreased volume) is observed in the head and body regions. **(b)** Correlation with compass slope scores. Positive correlation (increased volume) is observed in the head region and negative correlation (decreased volume) is observed in the body region.

4.3.2 Right Hippocampus

The right hippocampus was shown to predict the learning slopes in the compass task and the first training trial scores in the map task with 70% and 69.5% accuracy, respectively. The VBM results with the compass slope scores further revealed positive correlation in the body region of the right hippocampus (Figure 22a). This finding indicated that the participants with higher compass slope scores had larger gray matter volume in the body region of this structure. The correlation of the right hipocampus with the map 1 scores using the VBM demonstrated negative correlation in the tail region and positive correlation in the head region of this structure (Figure 22b). According to these results, faster participants in the initial map training trial had less gray matter volume in the tail of the right hippocampus and larger gray matter volume in the head of the right hippocampus.

4.3.3 Right Caudate

Classification results revealed a correlation between the right caudate and the scores obtained in the test trial of the map task with 73.5%. The VBM analysis using the map test scores revealed negative correlation in the head of the right caudate. (Figure 23) This result indicates that the better performers in the test trial of the map task had less gray matter volume in the head region of the right caudate.

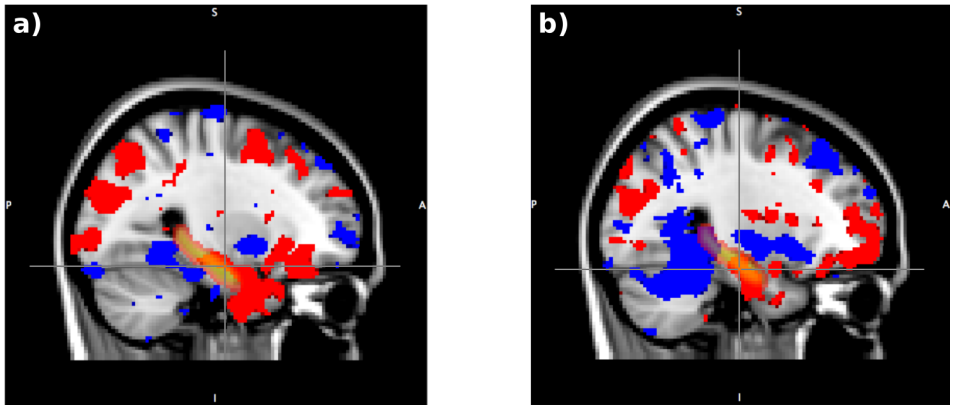

Figure 22: The VBM results (sagittal view) showing the positively (red) and negatively (blue) correlated volume changes shown on the right hippocampus (red-yellow) which was localized with Harvard subcortical structures atlas. **(a)** Correlation with compass slope scores. Positive correlation (increased volume) is observed in the body region and no negative correlation is apparent. **(b)** Correlation with map 1 scores. Positive correlation (increased volume) is observed in the tail region and negative correlation (decreased volume) is observed in the head region.

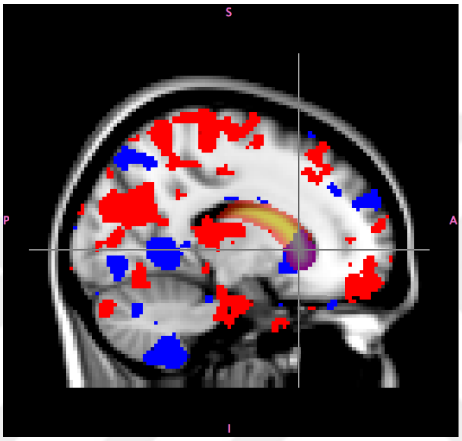

Figure 23: The VBM results with the test scores in the map task (sagittal view) showing the positively (red) and negatively (blue) correlated volume changes shown on the right caudate (red-yellow) which was localized with Harvard subcortical structures atlas. Negative correlation (decreased volume) is observed in the head of the right caudate.

4.4 Local Statistical Shape Analysis Results

Global statistical analysis using the VBM showed structures and regions that (positively and negatively) correlated with the behavioral tests that showed over 60% prediction accuracy in the classification results. Although these regions indicated differences in gray matter in these structures, precise localization cannot be achieved with the VBM. For this reason, local statistical analysis using SPHARM-PDM reconstructed images and the MANCOVA was also included in this study. These analyses revealed further localizations of the significantly correlated regions

on the hippocampus and the caudate along with the direction of the local shape changes. Here, vectors show the mean change from the bad navigators to good navigators in a particular test.[2] These results are presented with uncorrected p-values as the locally significant regions did not survive comparisons for multiple corrections.

4.4.1 Left Hippocampus

The correlation between the left hippocampus and the map slope scores revealed that the statistically significant areas were distributed around the tail and lower body regions. However, the shape changes in the tail and lower body of the left hippocampus were localized and showed predominantly dilations with a few scattered contractions (Figure 24a). In contrast, statistically significant areas were localized in the head and upper body regions of the left hippocampus and showed local contractions (Figure 24b). According to these results, the participants that showed better improvement during map task training trials had volume changes largely in the tail and the lower body of the left hippocampus. The results also demonstrated that the volume changes in these regions were predominantly dilations in these participants. On the contrary, the significantly correlated regions in the upper body and the head of the left hippocampus of these participants were localized and showed contractions.

The MANCOVA analysis with the left hippocampus and the compass slope scores demonstrated that the statistically significant areas were localized in both the tail and the head regions of the left hippocampus. Furthermore, the local shape changes occurring in these statistically significant areas were due to contractions in both regions (Figure 24c,d). These findings indicate that the participants that displayed better learning (i.e., sharper slope) during the training trials of the compass task had local contractions in the tail and the head regions of the left hippocampus.

[2]Vectors that do not originate from the statistically significant regions are considered as unrelated to the behavioral performances.

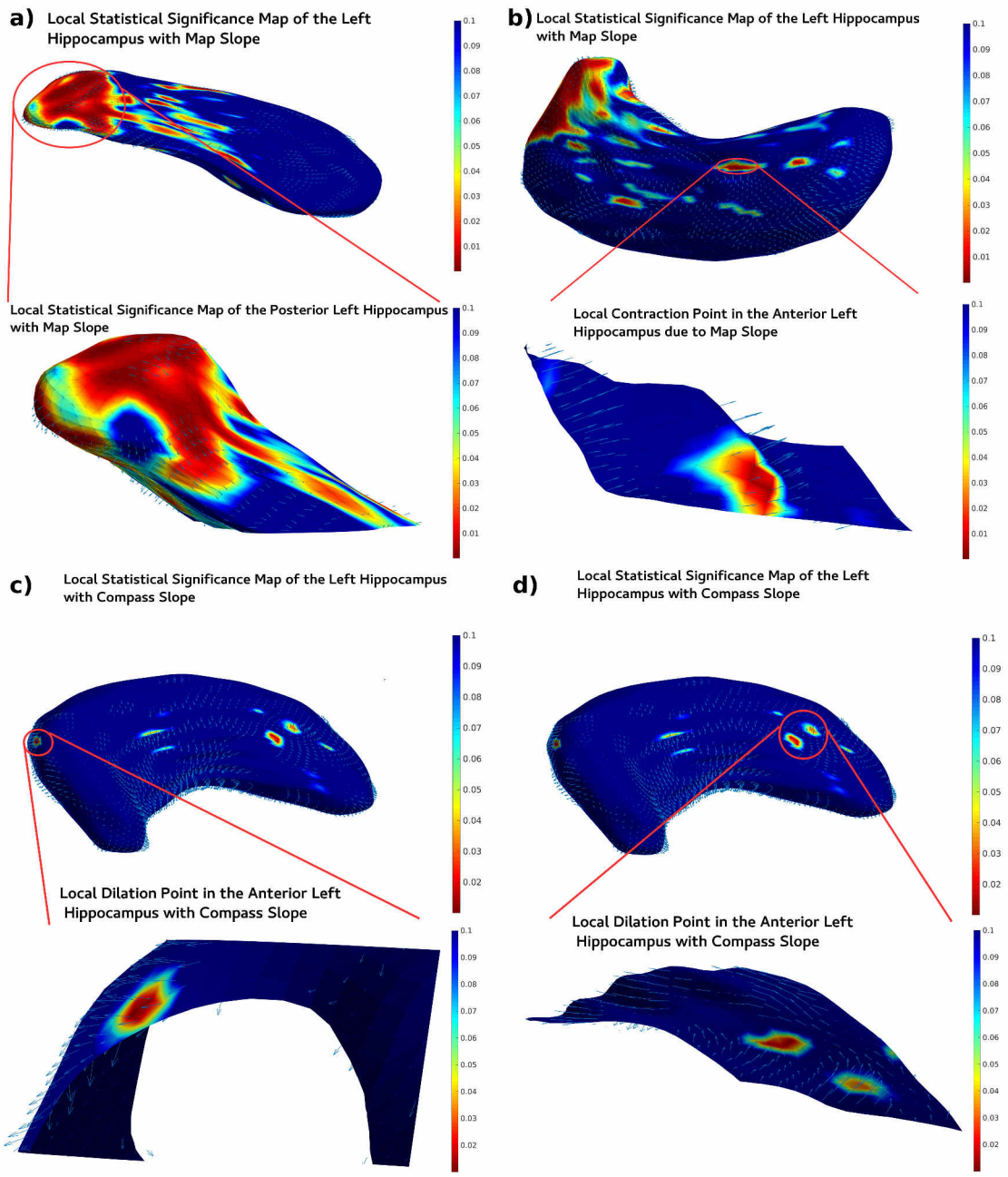

Figure 24: Local statistical significance map of the left hippocampus with the map slope scores **(a)** with a closer look on the tail region showing nonlocalized statistical significance but localized shape changes predominantly due to dilations and **(b)** with a closer look (from the inside) on the head region showing localized statistical significance and localized contractions. Local statistical significance map of the left hippocampus with the compass slope scores **(c)** with a closer look on the head and **(d)** on the tail regions both showing localized significance and localized dilations.

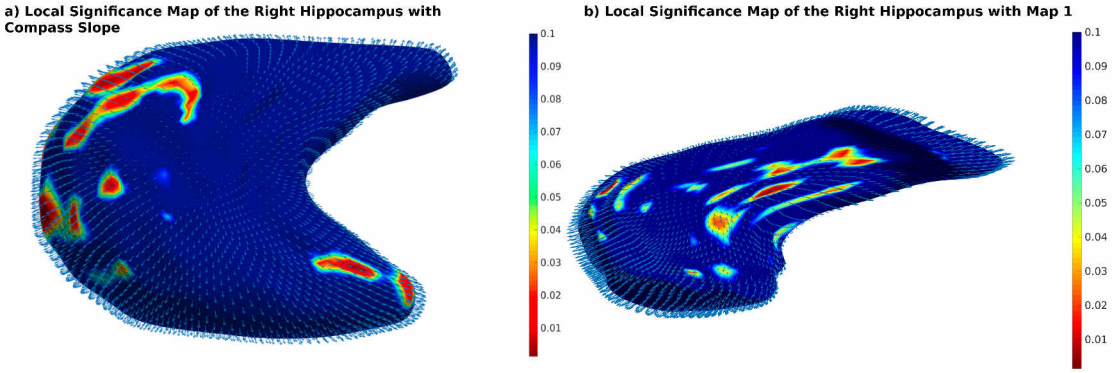

Figure 25: Local statistical significance map of the right hippocampus **(a)** with the compass slope scores showing localized statistical regions due to dilation in the head region and throughout the body region and **(b)** with the map 1 scores showing significant correlation and dilations predominantly in the body region.

4.4.2 Right Hippocampus

Preliminary classification results showed that the right hippocampus was correlated with the compass slope and the map 1 tasks. The MANCOVA analysis with the reconstructed right hippocampus (using SPHARM-PDM) and the compass slope scores revealed localized significant regions in the head region and throughout the body region. In addition, these local changes showed an increase in the volume (Figure 25a). These results indicated that the participants with a greater improvement over the response learning training trials had local dilations in the head and the body region of the right hippocampus.

The MANCOVA analysis on the right hippocampus with the first training trial scores of the map task demonstrated that the significantly correlated regions were concentrated in the body region. These statistically significant regions also showed an increase in the volume and no contraction was observed (Figure 25b). These results indicated that the better performers in the initial spatial training session had larger body in their right hippocampus as compared to the worse performers.

4.4.3 Right Caudate

In the classification results, the right caudate was shown to predict participants' scores on the test trial of the map task. The MANCOVA analysis further demonstrated that the significantly correlated regions were localized and scattered around the head region. Locally significant regions were also observed to result from a decrease in the gray matter volume (Figure 26). According to these results, participants that performed better during the test trial in the map task had smaller local regions in the head region of their caudate.

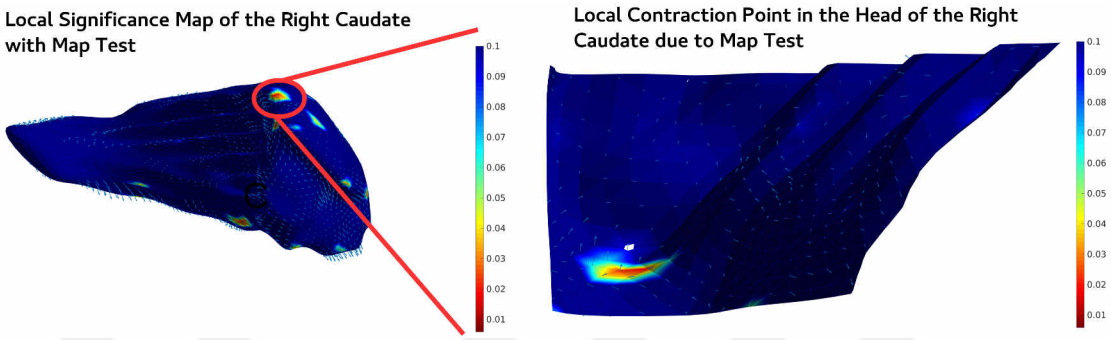

Figure 26: Local statistical significance map of the right caudate with the map test scores with a closer look on the head region (from the inside) showing localized statistical regions due to contractions in the head region.

5 Discussion

This Master's investigated the relationship between the place and response learning navigation systems using local shape features of the hippocampus and the caudate. To that end, data from an experiment in a virtual environment was used. This experiment consisted of two tasks that were specifically designed to recruit two navigation systems based on place and response learning. In the analysis, T1-weighted images of participants collected prior to the task were used to segment the hippocampus and the caudate. Local shape features of these structures were then extracted using the SPHARM method. Next, SPHARM coefficients were utilized in SVM classification to assess structures' ability to distinguish good and bad navigators (median separated) in three different aspects of each of the two navigation tasks. In addition, global and local statistical analyses were carried out using the VBM and the MANCOVA to determine regions that correlated with these six different aspects. This study demonstrated the ability of local

features of the hippocampus and the caudate to predict different aspects of spatial navigation. In addition, local statistical analysis based on these local features was shown to effectively localize the shape changes occurring in these structures. Therefore, this Master's thesis revealed the importance of local analysis in spatial navigation and provided a novel method for future research.

The VR experiment used in this study consisted of two tasks. In the compass task, participants were trained in five trials to follow a specific route indicated by an arrow and then reproduce the same route without the arrow in a test trial. In the map task, participants were required to find a target using a map during the training trials and then reach the target without the map in the test trial. In both tasks the time required by participants to reach the target during training and test trials were recorded in units of seconds. Furthermore, the slopes of lines fitted to training trial scores of compass and map tasks were utilized as a measure of response and place learning, respectively. In the analysis, participants' first training trial scores, learning slopes and test trial scores in both tasks were investigated.

Map slope scores were obtained from the slope of the participants' individual scores in map task training trials and participants that were able to develop novel routes to reach the target faster obtained higher score. Results from SVM classification demonstrated a correlation between the left hippocampus and the map slope scores with a 74.5% prediction accuracy. Furthermore, map slope scores were used in the global and local statistical analyses to validate this correlation. The findings from the VBM analysis showed that the tail of the left hippocampus had positive correlation with the slopes whereas the head of the left hippocampus had negative correlation. Local statistical analysis with the MANCOVA demonstrated that the significantly correlated regions in the tail and lower body of the left hippocampus were not locally distributed. However, the MANCOVA analysis also revealed that the shape changes in these regions were localized and showed predominantly dilations with a few scattered contractions. In contrast, the MANCOVA results in the head and upper body regions of the left hippocampus showed localized statistically significant areas due to local contractions.

Previous research has shown the importance of the hippocampus in tasks that require subjects to develop novel and flexible routes (Hartley et al., 2003; Bohbot et al., 2007; Marchette et al., 2011). Furthermore, previous studies has also demonstrated that the better place learners had larger gray matter volume in the tail of the right hippocampus and less gray matter volume in the head of the right hippocampus (Maguire et al., 2000; Schinazi et al., 2013). The findings from this study confirms the correlation between the participants' ability to develop novel routes and the left hippocampus. In addition, the statistical analyses carried out in this study demonstrate the same local shape changes in the head and tail regions of the left hippocampus but no significant correlation was found between the right hippocampus and the map slope scores (prediction accuracy 40%).

Another indicator of the participants' place learning abilities was the scores obtained in the test trial of the map task. In this trial, participants were required to find the target without using any navigation aid and to utilize the mental representations of the environment. Following the classification analysis, the right caudate was observed to predict map test results with 73.5% accuracy. While the classification results do not indicate whether the correlation is positive or negative, they confirm that there is a strong correlation between the right caudate and map test scores. The VBM analysis with participants map task test scores revealed that this correlation was negative and concentrated on the head region of the right caudate. Additional local statistical analysis using the MANCOVA demonstrated that these shape changes were substantially local and scattered around the head region. More specifically, these local changes were shown to be contractions in the gray matter volume. This finding builds on the VBM analysis by showing local changes in volume in the head of the right caudate as related to specific contractions.

Previous research has shown that the structural changes on the caudate nucleus in a place learning related task were correlated negatively with the behavioral scores (Hartley et al., 2003; Bohbot et al., 2007; Schinazi et al., 2013). In addition, previous studies has also demonstrated negative correlation in the head region of the right caudate nucleus (Hartley et al., 2003; Bohbot et al., 2007). The findings from this study are in alignment with the negative correlation observed in the head of the right caudate but also demonstrates the exact locations of contractions in the gray matter volume.

The initial training trial scores in the map task indicate the participants' ability to judge the relative direction of the goal from the map and establish spatial relations in order to find their ways in an unfamiliar environment using a map. For this reason, this task showed the capability of participants to make JRDs and to display efficient novel routes. Classification accuracies showed a correlation between the right hippocampus and the scores from the first training trial of the map task with a prediction accuracy of 69.5%. Additional VBM results with the initial map task training scores demonstrated negative correlation in the tail region of the hippocampus and positive correlation in the head and body regions of the right hippocampus. However, local statistical analysis results revealed significantly correlated regions only in the body regions which were due to local dilations and no contractions were observed.

In a previous study, Schinazi and colleagues (2013) have demonstrated the importance of the right hippocampus in making JRDs and developing mental shortcuts (Schinazi et al., 2013). The correlation observed in this study aligns with the role of the hippocampus in making JRDs in an unfamiliar environment. Furthermore, Packard and McGaugh (1996) showed that the place learning is recruited before the response learning (Packard and McGaugh, 1996). The correlation between the right hippocampus and the initial map task training trial scores also confirms the role of the hippocampus in the initial learning. However, the VBM results showing negative correlation in the tail of the right hippocampus contradicts with the previous studies that have shown positive correlation between the place learning tasks and the tail of the right hippocampus (Maguire et al., 2000; Schinazi et al., 2013).

In this study, positive correlations with the place learning were shown in the tail of the left hippocampus and the body of the right hippocampus and negative correlation with the place learning was observed in the head of the right caudate. This indicates that the recruitment of place learning system caused a structural degradation in the caudate. The relationship between the hippocampus and the caudate is investigated in the framework of Hartley and Burgess (2005) that proposes three possible interactions (Hartley and Burgess, 2005). Competition occurs when the hippocampus and the caudate drive conflicting responses during learning and they compete to control the behavior. Competitive interaction is manifested when structural degradation is observed in the caudate during place learning or in the hippocampus during response learning. Competition differs from cooperation and compensation that suggest positive interaction

in between. In this study, the correlation between the place learning and the hippocampus was observed to be positive whereas negative correlation was apparent in the caudate during place learning. Therefore, this study constitutes an example to competitive relationship between the hippocampus and the caudate.

The three different aspects from the compass task (initial training trial, learning slope and test results) were also investigated in this study but no correlation was found between the first training trial scores (max. accuracy 53.13% with the right hippocampus) and the test scores (max. accuracy 39.06% with the left caudate) and the hippocampus and the caudate. Therefore, only the compass slope scores were investigated.

Compass slope was calculated from the slopes of participants' scores in training trials in the compass task. For this reason, this measurement showed the participants' ability of learning a fixed route by following an arrow and was an indicator of response learning abilities. Classification results showed correlations between compass slope scores and the left and right hippocampus with prediction accuracies 70.15% and 70%, respectively. The compass slope scores were also used in the VBM which showed that these accuracies were due to positive correlations in the head of the left hippocampus and in the head and body regions of the right hippocampus. Local statistical analysis further revealed that statistically significant regions were localized in the head region of the left hippocampus and the head and body regions of the right hippocampus. In addition, these locally significant regions were observed to show local dilations, confirming the increase in the gray matter volume observed in the VBM.

No previous study has shown positive correlation between the ability of learning a fixed route and the hippocampus. These findings from this Master's work can be interpreted as latency in the response learning system. As shown by Packard and McGaugh (1996), place learning system is recruited earlier than the response learning system (Packard and McGaugh, 1996). For this reason, it is possible that the participants were using the mental representations during the arrow task training trials. Alternatively, it is possible to argue that the participants were learning the virtual environment and storing spatial information which caused the employment of the hippocampus.

In this study both global and local statistical analysis methods were employed. While the positive correlations observed in the VBM aligned with the dilations in the MANCOVA analysis, local statistical analysis was demonstrated to provide exact locations of shape changes. Therefore, local analysis method that depends on shape analysis and local shape descriptors was shown to provide deeper insight about the effects of behavioral tasks on cortical structures. Previous studies on human spatial navigation have used global statistical analysis methods (i.e., the VBM, the volumetry) in order to relate the behavioral performances to the volume changes on cortical structures. However, shape analysis methods (such as SPHARM) have been employed commonly in clinical diagnostic research. For these studies, local analysis methods provided enough discriminative power for construction of models to carry out an evaluation based on the anatomical properties of the cortical structures. In addition, the shape analysis methods also allowed for the visualization of localized gray matter volume changes. In this study, we have shown that a similar methodology can be applied in spatial navigation research. To that end, we also provided a pipeline for future spatial navigation research. According to our study, the local features of cortical structures are extracted using shape analysis methods and then used in machine learning algorithms to evaluate correlations. Furthermore, local statistical analysis is carried out using these local descriptors and can provide exact locations of shape changes that correlate with the behavioral tasks.

The main limitation of this study was the number of subjects that participated in the experiment. The type of statistical analyses used in this research can depend on the number of data available and small datasets can reduce statistical power. In this experiment, the total number of subjects were limited to 20 which is low even for neurological studies where the number of subjects typically range from 30 to 100 (Maguire et al., 2000; Gerardin et al., 2009). In addition, these participants had to be median separated into good and bad navigators for the application of classification algorithms. This reduced the members of each class to only ten. The small dataset affected the results in two main ways. First, small datasets introduce a very strong bias in machine learning applications. Therefore, this Masters study utilized a very pessimistic training algorithm (two-nested CV algorithm) in order to reduce the bias (Varma and Simon, 2006). Naturally, using a very pessimistic training method limited the true predictive power of strongly correlated combinations while distinguishing them from weakly correlated ones. Secondly, the reduced statistical power of having a small dataset is also apparent on both global and local statistical analyses. Results of both the VBM method and the MANCOVA method did not survive

comparison for multiple corrections and only the uncorrected p-values were presented. For this reason, the results of this study may not generalize.

Another limitation of this study is that the self evaluation questionnaires were not included. These questionnaires in spatial navigation research have been used to assess participants' abilities and tendencies to utilize mental representations and habitual responses (Schinazi et al., 2013). The results from these questionnaires can be correlated with behavioral performances to identify the underlying effects of the tasks. This study lacks the correlation between psychometric tests and the measured behavioral scores. For this reason, the indications of the behavioral scores used in this study were assumed and compared to the previous studies accordingly without knowing whether a particular place or response learning task is related to mental representations or habitual responses.

This Master's study provides a novel and a more precise way of investigating the neural correlates of place and response learning using shape analysis and machine learning methods. However, future research should consider some changes to the methodology and sampling. First,the dataset should include as much subjects as possible in order to avoid the intrinsic bias since the methodology is based on statistical learning and the effect of the dataset size is significant. The larger dataset would allow the researcher to carry out the machine learning analysis with less pessimistic approaches and to increase the statistical power in the global and local analyses. In addition, a personal assessment of participants' spatial cognition abilities would allow the researcher to carry out statistical analysis to see the correlation between the obtained behavioral results. This would allow the researcher to identify the underlying effects of the designed behavioral tasks and to interpret the results accordingly without any assumptions.

6 Conclusion

This Master's study used machine learning and shape analysis methods in order to investigate the role of the hippocampus and caudate in response and place learning. In addition, the present study provided a comparison between the global and local approaches. For the most part, the results suggest a competitive relationship between the hippocampus and the caudate. In particular, the tail of the left hippocampus and head of the right caudate showed significant positive and

negative correlation with place learning abilities. Furthermore, local statistical analysis provided deeper insight and revealed the exact locations and directions of structural changes. Therefore, this Master's work demonstrated the importance of local features of the hippocampus and the caudate and proposed a novel way for local investigation of cortical structures in future spatial navigation research.

7 References

[1] - Adamiak, K., Duch, P. and lot, K. (2016). Object Classification Using Support Vector Machines with Kernel-based Data Preprocessing. *Image Processing & Communications*, 21(3), pp.45-53.

[2] - Agranoff, D., Fernandez-Reyes, D., Papadopoulos, M., Rojas, S., Herbster, M., Loosemore, A., Tarelli, E., Sheldon, J., Schwenk, A., Pollok, R., Rayner, C. and Krishna, S. (2006). Identification of diagnostic markers for tuberculosis by proteomic fingerprinting of serum. *The Lancet*, 368(9540), pp.1012-1021.

[3] - Ambroise, C. and McLachlan, G. (2002). Selection bias in gene extraction on the basis of microarray gene-expression data. *Proceedings of the National Academy of Sciences*, 99(10), pp.6562-6566.

[4] - Andersson, M. Jenkinson and S. Smith (2007) Non-linear registration, aka Spatial normalisation. FMRIB technical report TR07JA2 from www.fmrib.ox.ac.uk/analysis/techrep

[5] - Bohbot, V., Lerch, J., Thorndycraft, B., Iaria, G. and Zijdenbos, A. (2007). Gray Matter Differences Correlate with Spontaneous Strategies in a Human Virtual Navigation Task.*Journal of Neuroscience*, 27(38), pp.10078-10083.

[6] - Brechbühler, C., Gerig, G. and Kbler, O. (1995). Parametrization of Closed Surfaces for 3-D Shape Description.*Computer Vision and Image Understanding*, 61(2), pp.154-170. Brechbühler et al., 1995

[7] - Buzsaki, G. (2005). Theta rhythm of navigation: Link between path integration and landmark navigation, episodic and semantic memory. *Hippocampus*, 15(7), pp.827-840.

[8] - Cawley, G. and Talbot, N. (2010). On Over-fitting in Model Selection and Subsequent Selection Bias in Performance Evaluation. *Journal of Machine Learning Research*.

[9] - Chan, H., Li, H. and Lui, L. (2016). Quasi-conformal statistical shape analysis of hippocampal surfaces for Alzheimers disease analysis.*Neurocomputing*, 175, pp.177-187.

[10] - Crowther, P.S. and Cox, R.J. (2005). A Method for Optimal Division of Data Sets for Use in Neural Networks. *Lecture Notes in Computer Science Knowledge-Based Intelligent Information and Engineering Systems*, pp.17.

[11] - Cortes, C. and Vapnik, V. (1995). Support-vector networks. *Machine Learning*, 20(3), pp.273-297.

[12] - Delpolyi, A., Rankin, K., Mucke, L., Miller, B. and Gorno-Tempini, M. (2007). Spatial cognition and the human navigation network in AD and MCI.*Neurology*, 69(10), pp.986-997.

[13] - Douaud G., Smith S., Jenkinson M., Behrens T., Johansen-Berg H., Vickers J., James S., Voets N., Watkins K., Matthews P.M and, James A. (2007) Anatomically related grey and white matter abnormalities in adolescent-onset schizophrenia. *Brain* 130:2375-2386.

[14] - Douglas, R. (1967). The hippocampus and behavior. *Psychological Bulletin*, 67(6), pp.416-442.

[15] - Ekstrom, A., Caplan, J., Ho, E., Shattuck, K., Fried, I. and Kahana, M. (2005). Human hippocampal theta activity during virtual navigation.*Hippocampus*, 15(7), pp.881-889.

[16] - Ekstrom, A., Kahana, M., Caplan, J., Fields, T., Isham, E., Newman, E. and Fried, I. (2003). Cellular networks underlying human spatial navigation.*Nature*, 425(6954), pp.184-188

[17] - Ertmer, P. and Newby, T. (1993). Behaviorism, Cognitivism, Constructivism: Comparing Critical Features from an Instructional Design Perspective.*Performance Improvement Quarterly*, 6(4), pp.50-72.

[18] - Fedorov A., Beichel R., Kalpathy-Cramer J., Finet J., Fillion-Robin J-C., Pujol S., Bauer C., Jennings D., Fennessy F.M., Sonka M., Buatti J., Aylward S.R., Miller J.V., Pieper S., Kikinis R. 3D Slicer as an Image Computing Platform for the Quantitative Imaging Network. *Magnetic Resonance Imaging*. 2012 Nov;30(9):1323-41. PMID: 22770690. PMCID: PMC3466397.

[19] - Gerardin, E., Chtelat, G., Chupin, M., Cuingnet, R., Desgranges, B., Kim, H., Niethammer, M., Dubois, B., Lehricy, S., Garnero, L., Eustache, F. and Colliot, O. (2009). Multidimensional classification of hippocampal shape features discriminates Alzheimer's disease and mild cognitive impairment from normal aging.*NeuroImage*, 47(4), pp.1476-1486.

[20] - Gerig G., Styner M., Jones D., Weinberger D., Lieberman J. (2001). Shape analysis of brain ventricles using SPHARM. *Proceedings IEEE Workshop on Mathematical Methods in Biomedical Image Analysis* (MMBIA 2001).

[21] - Good C.D., Johnsrude I.S., Ashburner J., Henson R.N., Friston K.J., Frackowiak R.S. (2001) A voxel-based morphometric study of ageing in 465 normal adult human brains. *Neuroimage*.14:21-36.

[22] - Grübel J. Assessing Human Interface Device Interaction in Virtual Environments [Bachelor Thesis]. ETH Zürich; 2014. Available from: http://e-collection.library.ethz.ch/view/eth:48223.

[23] - Gutman, B., Wang, Y., Morra, J., Toga, A. and Thompson, P. (2009). Disease classification with hippocampal shape invariants. *Hippocampus*, 19(6), pp.572-578.

[24] - Guyon, I., Wetson, J., Barnhill, S. and Vapnik, V. (2002). Gene Selection for Cancer Classification using Support Vector Machines. *Machine Learning*, 46, pp.389-422.

[25] - Hafting, T., Fyhn, M., Molden, S., Moser, M. and Moser, E. (2005). Microstructure of a spatial map in the entorhinal cortex. *Nature*, 436(7052), pp.801-806.

[26] - Hartley, T. and Burgess, N. (2005). Complementary memory systems: competition, co-operation and compensation.*Trends in Neurosciences*, 28(4), pp.169-170. Hartley and Burgess, 2005

[27] - Hartley, T. and Harlow, R. (2012). An association between human hippocampal volume and topographical memory in healthy young adults.*Frontiers in Human Neuroscience*, 6.

[28] - Hartley, T., Maguire, E., Spiers, H. and Burgess, N. (2003). The Well-Worn Route and the Path Less Traveled.*Neuron*, 37(5), pp.877-888.

[29] - Hassabis, D., Chu, C., Rees, G., Weiskopf, N., Molyneux, P. and Maguire, E. (2009). Decoding Neuronal Ensembles in the Human Hippocampus.*Current Biology*, 19(7), pp.546-554.

[30] - Hsu C. and Lin C. (2002). A comparison of methods for multiclass support vector machines. *IEEE Transactions on Neural Networks*, 13(2), pp.415-425.

[31] - Huang, M., Hung, Y., Lee, W., Li, R. and Jiang, B. (2014). SVM-RFE Based Feature Selection and Taguchi Parameters Optimization for Multiclass SVM Classifier.*The Scientific World Journal*, 2014, pp.1-10.

[32] - Iaria, G., Petrides, M., Dagher, A., Pike, B. and Bohbot, V. (2003). Cognitive Strategies Dependent on the Hippocampus and Caudate Nucleus in Human Navigation: Variability and Change with Practice.*The Journal of Neuroscience*, 23(13), pp.5945-5952.

[33] - Jacobs, J. (2013). Hippocampal theta oscillations are slower in humans than in rodents: implications for models of spatial navigation and memory.*Philosophical Transactions of the Royal Society B: Biological Sciences*, 369(1635), pp.20130304-20130304.

[34] - Jacobs, J., Weidemann, C., Miller, J., Solway, A., Burke, J., Wei, X., Suthana, N., Sperling, M., Sharan, A., Fried, I. and Kahana, M. (2013). Direct recordings of grid-like neuronal activity in human spatial navigation.*Nature Neuroscience*, 16(9), pp.1188-1190.

[35] - Jenkinson M., Bannister P.R., Brady, J.M., and Smith S.M. (2002). Improved optimisation

for the robust and accurate linear registration and motion correction of brain images.*NeuroImage*, 17(2):825-841.

[36] - Jenkinson M., Beckmann C.F., Behrens T.E., Woolrich M.W., Smith S.M. (2012). FSL. *NeuroImage*, 62:782-90.

[37] - Jenkinson M. and Smith S.M.. A global optimisation method for robust affine registration of brain images. *Medical Image Analysis*, 5(2):143-156, 2001.

[38] - Kahana, M., Sekuler, R., Caplan, J., Kirschen, M. and Madsen, J. (1999). Human theta oscillations exhibit task dependence during virtual maze navigation.*Nature*, 399(6738), pp.781-784.

[39] - Kavzoglu, T. and Colkesen, I. (2009). A kernel functions analysis for support vector machines for land cover classification.*International Journal of Applied Earth Observation and Geoinformation*, 11(5), pp.352-359.

[40] - Keerthi, S. (2002). Efficient tuning of SVM hyperparameters using radius/margin bound and iterative algorithms. *IEEE Transactions on Neural Networks*, 13(5), pp.1225-1229.

[41] - Kimble, D. (1968). Hippocampus and internal inhibition. *Psychological Bulletin*, 70(5), pp.285-295.

[42] - Lerman, P. (1980). Fitting Segmented Regression Models by Grid Search. *Applied Statistics*, 29(1), p.77.

[43] - Li, S., Shi, F., Pu, F., Li, X., Jiang, T., Xie, S. and Wang, Y. (2007). Hippocampal Shape Analysis of Alzheimer Disease Based on Machine Learning Methods.*American Journal of Neuroradiology*, 28(7), pp.1339-1345.

[44] - Liu, L., Liu, B., Huang, H. and Bovik, A. (2014). No-reference image quality assessment based on spatial and spectral entropies. *Signal Processing: Image Communication*, 29(8), pp.856-863.

[45] - Lorensen, W. and Cline, H. (1987). Marching cubes: A high resolution 3D surface construction algorithm. *ACM SIGGRAPH Computer Graphics*, 21(4), pp.163-169.

[46] - Maguire, E., Gadian, D., Johnsrude, I., Good, C., Ashburner, J., Frackowiak, R. and Frith, C. (2000). Navigation-related structural change in the hippocampi of taxi drivers. *Proceedings of the National Academy of Sciences*, 97(8), pp.4398-4403.

[47] - Maguire, E., Spiers, H., Good, C., Hartley, T., Frackowiak, R. and Burgess, N. (2003). Navi-

gation expertise and the human hippocampus: A structural brain imaging analysis.*Hippocampus*, 13(2), pp.250-259.

[48] - Maguire, E., Woollett, K. and Spiers, H. (2006). London taxi drivers and bus drivers: A structural MRI and neuropsychological analysis.*Hippocampus*, 16(12), pp.1091-1101.

[49] - Mahmoudi, A., Takerkart, S., Regragui, F., Boussaoud, D. and Brovelli, A. (2012). Multi-voxel Pattern Analysis for fMRI Data: A Review.*Computational and Mathematical Methods in Medicine*, 2012, pp.1-14.

[50] - Maimon, O. and Rokach, L. (2010). *Data mining and knowledge discovery handbook*. New York: Springer, pp.231-247.

[51] - Mandler, G. (2011). *A history of modern experimental psychology.* Cambridge, Mass.: MIT Press.

[52]- Marchette, S., Bakker, A. and Shelton, A. (2011). Cognitive Mappers to Creatures of Habit: Differential Engagement of Place and Response Learning Mechanisms Predicts Human Navigational Behavior.*Journal of Neuroscience*, 31(43), pp.15264-15268.

[53] - Miller, G. (2003). The cognitive revolution: a historical perspective.*Trends in Cognitive Sciences*, 7(3), pp.141-144.

[54] - Morgan, L., MacEvoy, S., Aguirre, G. and Epstein, R. (2011). Distances between Real-World Locations Are Represented in the Human Hippocampus.*Journal of Neuroscience*, 31(4), pp.1238-1245.

[55] - Morris, R. (1984). Developments of a water-maze procedure for studying spatial learning in the rat. *Journal of Neuroscience Methods*, 11(1), pp.47-60.

[56] - Moser, E., Kropff, E. and Moser, M. (2008). Place Cells, Grid Cells, and the Brain's Spatial Representation System.*Annual Review of Neuroscience*, 31(1), pp.69-89.

[57] - Muller, R. (1996). A Quarter of a Century of Place Cells. *Neuron*, 17(5), pp.813-822.

[58] - Nedelska, Z., Andel, R., Laczo, J., Vlcek, K., Horinek, D., and Lisy, J. et al. (2012). Spatial navigation impairment is proportional to right hippocampal volume. *Proceedings Of The National Academy Of Sciences*, 109(7), 2590-2594.

[59] - Neisser, U. (1967).*Cognitive psychology.* New Jersey: Prentice Hall.

[60] - Niedermeyer, E. and Da Silva, F. (2005). *Electroencephalography.* Philadelphia: Lippincott williams and wilkins.

[61] - O'Keefe, J. and Dostrovsky, J. (1971). The hippocampus as a spatial map. Preliminary evidence from unit activity in the freely-moving rat. *Brain Research*, 34(1), pp.171-175.

[62] - Packard, M. and McGaugh, J. (1996). Inactivation of Hippocampus or Caudate Nucleus with Lidocaine Differentially Affects Expression of Place and Response Learning.*Neurobiology of Learning and Memory*, 65(1), pp.65-72.

[63] - Packard, M., Hirsh, R. and White, N. (1989). Differential effects of fornix and caudate nucleus lesions on two radial maze tasks: evidence for multiple memory systems.*The Journal of Neuroscience*, 9(5), pp.1465-1472.

[64] - Paniagua, B., Styner, M., Macenko, M., Pantazis, D. and Niethammer, M. (2009). Local Shape Analysis using MANCOVA.*Insight*.

[65] - Pascal, L., Pedromo, J., Styner, M., Shah, H., and Paniagua, B. (2017) SPHARM-PDM User Tutorial. *The University of North Carolina*.

[66] - Patenaude, B., Smith, S.M., Kennedy, D., and Jenkinson M. (2011) A Bayesian Model of Shape and Appearance for Subcortical Brain. *NeuroImage*, 56(3):907-922

[67] - Restle, F. (1957). Discrimination of cues in mazes: A resolution of the "place-vs.-response" question.*Psychological Review*, 64(4), pp.217-228.

[68] - Saeys, Y., Inza, I. and Larranaga, P. (2007). A review of feature selection techniques in bioinformatics. *Bioinformatics*, 23(19), pp.2507-2517.

[69] - Schinazi, V., Nardi, D., Newcombe, N., Shipley, T. and Epstein, R. (2013). Hippocampal size predicts rapid learning of a cognitive map in humans. *Hippocampus*, 23(6), pp.515-528.

[70] - Skinner, B. (1953).*Science and human behavior*. New York: Free Press.

[71] - Slicer.org. (2018). *3D Slicer*. [online] Available at: https://www.slicer.org/ [Accessed 24 Aug. 2018].

[72] - Smith S.M. (2002).Fast robust automated brain extraction.*Human Brain Mapping*, 17(3):143-155.

[73] - Smith S.M., Jenkinson M., Woolrich M.W., Beckmann C.F., Behrens T.E.J., Johansen-Berg H., Bannister P.R., De Luca M., Drobnjak I., Flitney D.E., Niazy R., Saunders J., Vickers J., Zhang Y., De Stefano N., Brady J.M. and Matthews P.M. (2004). Advances in functional and structural MR image analysis and implementation as FSL. *NeuroImage*, 23(S1):208-19.

[74] - Solstad, T., Boccara, C., Kropff, E., Moser, M. and Moser, E. (2008). Representation of

Geometric Borders in the Entorhinal Cortex. *Science*, 322(5909), pp.1865-1868.

[75] - Stone, M. (1974). Cross-Validatory Choice and Assessment of Statistical Predictions. *Journal of the Royal Statistical Society. Series B (Methodological)*., Vol. 36(No. 2), pp.111-147.

[76] - Styner, M., Oguz, I., Xu, S., Brechbühler, C., Pantazis, D., Levitt, J., Shenton, M. and Gerig, G. (2006). Framework for the Statistical Shape Analysis of Brain Structures using SPHARM-PDM.*Insight*, (1071), pp.242-250.

[77] - Suk, H., Lee, S. and Shen, D. (2014). Hierarchical feature representation and multimodal fusion with deep learning for AD/MCI diagnosis.*NeuroImage*, 101, pp.569-582.

[78] - Suthana, N., Ekstrom, A., Moshirvaziri, S., Knowlton, B. and Bookheimer, S. (2009). Human Hippocampal CA1 Involvement during Allocentric Encoding of Spatial Information.*Journal of Neuroscience*, 29(34), pp.10512-10519.

[79] - Szekely, G., Kelemen, A., Brechbühler, C. and Gerig, G. (1996). Segmentation of 2-D and 3-D objects from MRI volume data using constrained elastic deformations of flexible Fourier contour and surface models.*Medical Image Analysis*, 1(1), pp.19-34.

[80] - Taube, J., Muller, R. and Ranck, J. (1990). Head-direction cells recorded from the postsubiculum in freely moving rats. I. Description and quantitative analysis. *The Journal of Neuroscience*, 10(2), pp.420-435.

[81] - Tolman, E. (1948). Cognitive maps in rats and men.*Psychological Review*, 55(4), pp.189-208.

[82] - Varma, S. and Simon, R. (2006). Bias in error estimation when using cross-validation for model selection.*BMC Bioinformatics*, 7(1), p.91.

[83] - Vass, L., Copara, M., Seyal, M., Shahlaie, K., Farias, S., Shen, P. and Ekstrom, A. (2016). Oscillations Go the Distance: Low-Frequency Human Hippocampal Oscillations Code Spatial Distance in the Absence of Sensory Cues during Teleportation.*Neuron*, 89(6), pp.1180-1186.

[84] - Vass, L. and Epstein, R. (2016). Common Neural Representations for Visually Guided Reorientation and Spatial Imagery.*Cerebral Cortex*, p.bhv343.

[85] - Vlcek, K. and Laczo, J. (2014). Neural Correlates of Spatial Navigation Changes in Mild Cognitive Impairment and Alzheimer's Disease.*Frontiers in Behavioral Neuroscience*, 8.

[86] - Voermans, N., Petersson, K., Daudey, L., Weber, B., van Spaendonck, K., Kremer, H. and Fernndez, G. (2004). Interaction between the Human Hippocampus and the Caudate Nucleus

during Route Recognition.*Neuron*, 43(3), pp.427-435.

[87] - Watanabe, S., Blaisdell, A. and Huber, L. (2009).*Rational animals,irrational humans.* Tokyo: Keio University Centre for Advanced Research on Logic and Sensibility.

[88] - Watson, J. (1913). Psychology as the behaviorist views it. *Psychological Review*, 20(2), pp.158-177.

[89] - Woolrich M.W., Jbabdi S., Patenaude B., Chappell M., Makni S., Behrens T., Beckmann C., Jenkinson M., Smith S.M. (2009). Bayesian analysis of neuroimaging data in FSL. *NeuroImage*, 45:S173-86.

Appendices

A Mathematical Foundations of the SVM

SVM tries to fit a hyperplane with maximum margin in a multidimensional feature space (or transformed feature space) that splits the training data while maximizing the distance of nearest cleanly split training data to the hyperplane. Let the equation of the hyperplane be $< \vec{w}, \vec{x} > +b = 0$. Then the question of finding the optimal hyperplane is constructed by two arguments;

(i) The margin between two different classes needs to be maximized.

(ii) No data from either one of the classes may lie inside the margin.

These properties can be mathematically formulated for a d-dimensional feature space as follows;

$$max_{\vec{w}\in\Re^d, b\in\Re} \frac{2}{||\vec{w}||} \quad \text{or} \quad min_{\vec{w}\in\Re^d, b\in\Re} \frac{1}{2}||\vec{w}||^2, \qquad \text{maximization of the margin} \tag{10a}$$

$$\text{subject to} \quad y_i(< \vec{w}, \vec{x_i} > +b) \geq 1, \forall i \in 1, \ldots, n, \qquad \text{no data inside margin} \tag{10b}$$

where $\vec{w}$ is the normal vector to the hyperplane, b is the offset, $\vec{x_i}$ are the training data points, the y_i are the respective labels and n is the total number of data. In order to solve the optimization problem given in Eq.(10), Lagrange multipliers method is formed as given below;

$$\mathcal{L}(\vec{w}, b, \alpha) = \frac{1}{2}||\vec{w}||^2 - \sum_{i=1}^{n} \alpha_i (y_i(< \vec{w}, \vec{x}_i + b) - 1) \tag{11}$$

which is to be minimized with respect to variables α and b, resulting in the following characteristics;

$$\frac{\partial}{\partial b}\mathcal{L} = 0 \Rightarrow \sum_{i=1}^{n} y_i \alpha_i = 0 \qquad \frac{\partial}{\partial \vec{w}}\mathcal{L} = 0 \Rightarrow \vec{w} - \sum_{i=1}^{n} y_i \alpha_i \vec{x}_i = 0 \tag{12a}$$

Therefore, Eq.(11) states that the optimal hyperplane can be written as a linear combination of training data in the feature space and only training vectors with non-zero Lagrange multipliers have contribution to the optimal hyperplane. The training data with non-zero Lagrange multipliers are the ones that lie at the boundary of the margin and are known as the support vectors. The decision function of classification becomes as given Eq. (12)) below;

$$f(\vec{x}) = sgn(< \vec{w}, \vec{x} > +b) \tag{13}$$

B Classification Flowcharts

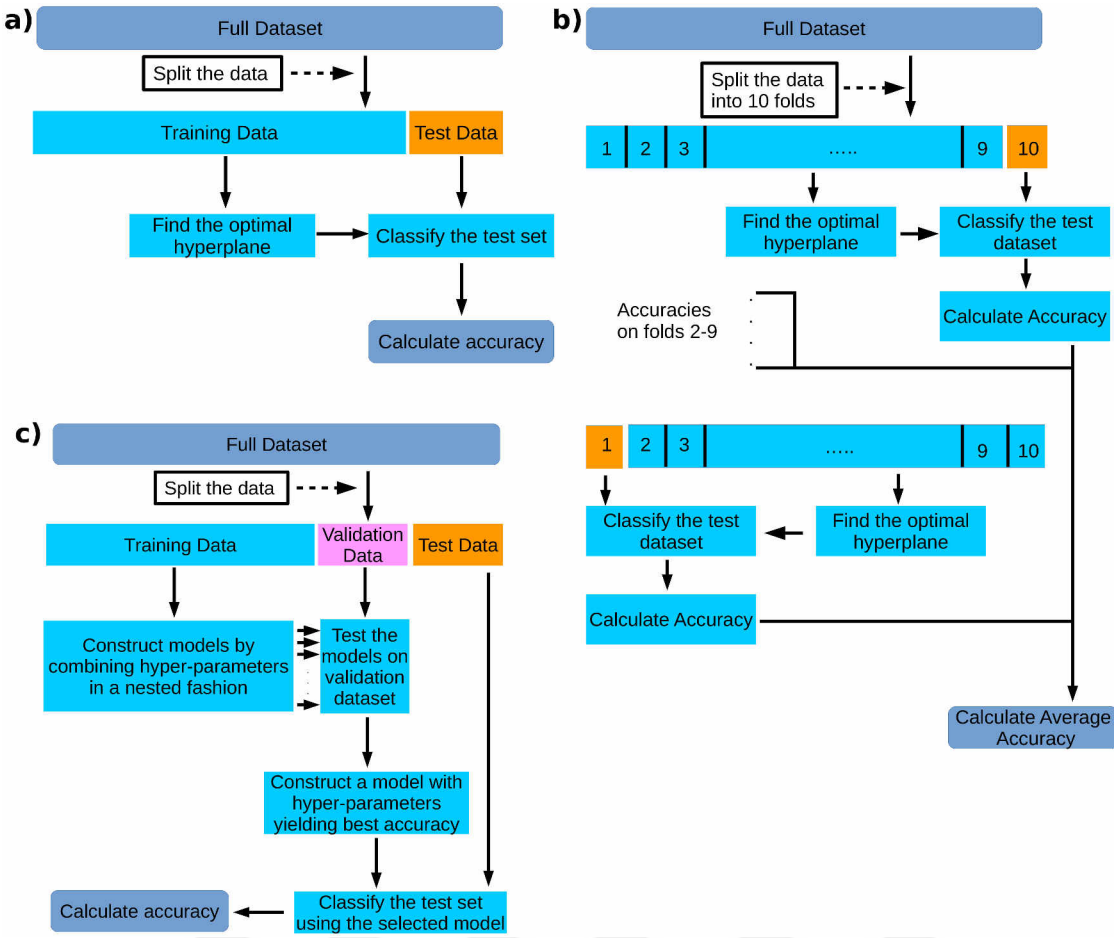

Figure 27: **(a)** Flowchart of basic classifier training with performance evaluation. The dataset is split into training and test sets with more data on the training set. The classifier is trained on training set and is then evaluated on test set. **(b)** Flowchart of classifier training with performance evaluation using CV. The dataset is split into k different folds (here, 10). The algorithm rotates k times to use each fold as test set while the classifier is trained with the remaining k-1 folds. The performance of the classifier is given by the averaging the accuracies obtained the evaluations on all test folds. **(c)** Flowchart of a classifier with performance evaluation and model selection. The dataset is divided into three. The training data is used to train classifiers with different model parameters and the performance of these models are tested on the validation set. Highest accuracy model is then applied to the test set and shows the performance of the classifier

C Complete Tables of Behavioral Scores

Training 1	Training 2	Training 3	Training 4	Training 5	Test	Slope
39.51	35.12	30.86	30.17	27.65	28.62	-2.87
50.79	53.84	47.54	47.35	41.96	45.65	-2.41
28.81	23.99	23.72	27.61	23.73	26.66	-0.22
33.85	33.89	32.97	31.07	28.31	54.57	-1.39
28.10	26.90	24.04	25.14	22.79	22.32	-1.24
36.86	36.38	34.65	32.39	28.11	49.87	-2.15
41.59	43.15	37.91	42.47	39.15	62.54	-0.56
30.30	28.23	28.01	27.51	28.02	32.45	-0.53
82.45	63.86	57.61	54.89	54.29	69.27	-6.53
38.86	32.16	30.48	31.98	29.31	31.58	-1.93
26.63	23.97	23.95	23.72	24.17	23.13	-0.52
76.54	63.31	62.95	51.91	58.35	43.16	-4.78
31.88	25.41	25.80	22.12	20.95	34.86	-2.52
31.90	32.69	35.70	36.61	33.69	44.37	0.75
74.99	71.57	69.62	71.38	61.40	69.51	-2.74
25.68	80.91	50.36	52.43	49.67	50.28	1.95
74.47	76.13	71.39	63.84	79.34	60.97	-0.26
51.43	44.63	45.17	43.86	45.00	68.65	-1.36
40.92	39.51	37.97	41.27	40.60	53.16	0.11
63.21	57.44	57.33	55.73	53.69	51.53	-2.08

Table 3: Participants' completion time in training and test trials in units of seconds, as well as computed learning slopes in compass task

Training 1	Training 2	Training 3	Training 4	Training 5	Test	Slope
72.47	25.14	19.36	18.01	17.19	16.58	-11.77
77.77	34.48	15.24	14.15	14.42	12.95	-14.70
49.38	20.09	14.53	13.03	13.11	13.05	-7.96
102.08	48.65	76.59	38.20	20.25	15.82	-17.41
38.56	39.51	26.61	18.23	13.78	13.33	-7.08
42.92	26.85	16.09	13.29	13.79	14.66	-7.18
62.70	27.62	22.14	23.66	20.12	24.89	-8.91
22.31	13.72	14.08	12.79	13.47	16.35	-1.86
53.29	60.77	36.46	31.11	30.34	29.85	-7.55
182.03	131.31	56.48	54.29	69.84	34.04	-30.14
35.15	15.15	13.73	12.72	11.72	11.99	-4.93
120.00	125.16	61.64	52.29	28.04	19.28	-25.68
59.33	17.11	13.54	15.34	12.98	13.99	-9.45
87.86	30.54	60.36	17.79	19.22	15.31	-15.00
90.01	41.83	28.40	23.76	20.24	20.58	-15.76
49.12	72.02	29.08	16.94	15.33	16.62	-12.27
166.61	138.32	143.92	107.11	86.53	35.26	-19.14
86.65	30.53	21.30	20.85	17.30	23.25	-14.84
183.25	123.57	23.44	19.30	17.97	18.56	-43.48
73.47	29.39	20.08	18.09	18.37	29.52	-12.15

Table 4: Participants' completion time in training and test trials in units of seconds, as well as computed learning slopes in map task

D Complete Classification Results

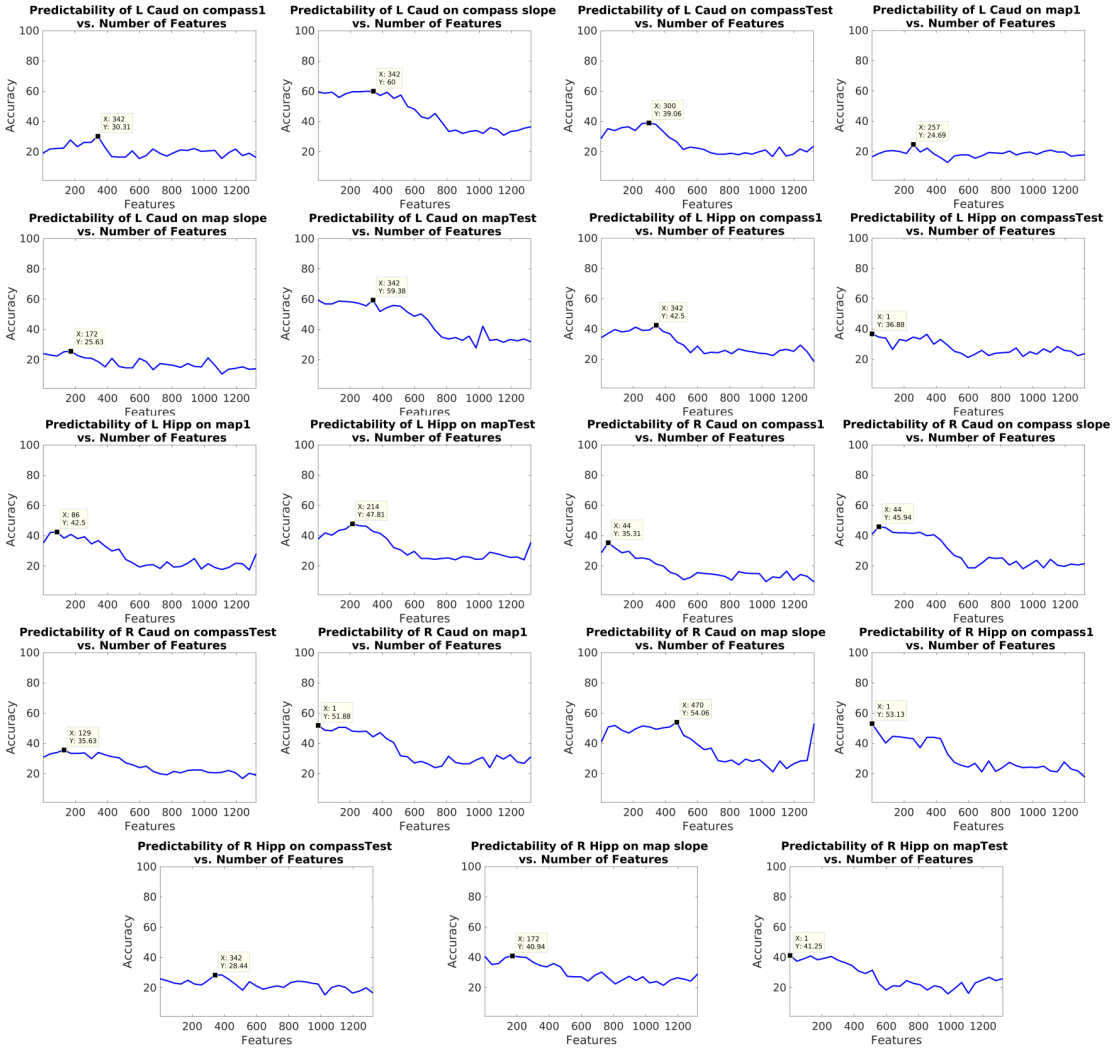

Figure 28: Prediction accuracy vs. number of features with structure test combination with 60% prediction accuracy or less (regarded as non-significant in this study).